UNIVERSIDADE DE LISBOA

FACULDADE DE CIÊNCIAS

DEPARTAMENTO DE FÍSICA

Delayed Enhancement cardiac MRI: reduction of image artefacts in patients with irregular heart rate

Andreia Calisto de Freitas

Dissertação

Mestrado Integrado em Engenharia Biomédica e Biofísica

Perfil de Radiações em Diagnóstico e Terapia

2013

UNIVERSIDADE DE LISBOA

FACULDADE DE CIÊNCIAS

DEPARTAMENTO DE FÍSICA

Delayed Enhancement cardiac MRI: reduction of image artefacts in patients with irregular heart rate

Andreia Calisto de Freitas

Dissertação

Mestrado Integrado em Engenharia Biomédica e Biofísica

Perfil de Radiações em Diagnóstico e Terapia

Orientador externo: Professor Doutor Tobias Schaeffter, KCL

Orientador interno: Professora Doutora Rita Nunes, IBEB, FCUL

2013

Resumo

DE-MRI (do inglês *delayed enhancement magnetic resonance imaging)* consiste numa técnica de imagiologia de ressonância magnética (MRI do inglês *Magnetic Resonance Imaging*) com especial aplicação em patologias cardíacas.

Nos últimos anos, as técnicas de imagiologia de ressonância magnética tem desempenhado um importante papel no diagnóstico e prognóstico médico. Características vantajosas tais como uma elevada resolução espacial, ausência de radiação ionizante e múltiplas aplicações impulsionaram o seu uso alargado a várias áreas da medicina moderna.

DE-MRI foi inicialmente desenvolvido para diagnóstico e avaliação de enfarctes do miocárdio (vulgarmente denominado *ataque de coração*). No entanto, a aplicaçao a doenças isquémicas não é exclusíva, sendo que recentes estudos demonstraram a sua utilidade no diagnóstico de outras patologias cardíacas tais como metástases cardíacas, infecções virais e condições genéticas.

DE-MRI consiste geralmente na aquisição de imagens com ponderação em T1 utilizando uma sequência IR (do inglês *inversion recovery*) após injeção de um agente de contraste. Tal como o nome indica *delayed enhancement* distingue-se das técnicas imagiológicas de contraste usuais uma vez que o momento de aquisição é atrasado por um determinado período de tempo (geralmente entre 10 a 20 min) após injeção do agente de contraste.

O agente de contraste mais frequente em DE-MRI é um composto à base de gadolíneo (Gd) chamado DTPA-Gd (do inglês *diethylene-triamine-penta-acid gadolinium*). O gadolíneo puro apresenta fortes características paramagnéticas, magnetizando-se quando sob o efeito de um campo magnético exterior, sendo por isso natural a sua utilização como agente de contraste em MRI. A utilização de um agente de contraste permite obter contraste de sinal entre determinados tecidos através de um efeito de redução dos tempos de

relaxação T1 dos protões circundantes. No entanto, é um composto altamente bio-tóxico e instável, sendo necessária a sua quelação com o composto DTPA para o tornar seguro em aplicações médicas.

Contudo, essa quelação leva a que as moléculas de Gd apresente um elevado tamanho molecular, tendo por isso tendência a acumular em tecidos que sofreram enfarte (tecido necrótico) uma vez que estes possuem um alargado espaço extracelular em oposição ao miocárdio saudável.

Devido a esta distribuição distinta do agente de contraste pelos tecidos cardíacos é possível obter o contraste de sinal entre o miocárdio que sofreu enfarcte e o saudável. Isto porque aquando o momento de aquisição, após o período de atraso, o agente de contraste já terá sido eliminado dos tecidos saudáveis mas ainda permanece em elevadas concentrações nos tecidos que sofreram enfarcte. Assim, a presença do Gd em maior concentração nestes tecidos irá reduzir o tempo de relaxação T1, reflectindo-se numa elevada intensitade de sinal em imagens com ponderação T1.

Resumindo, numa imagem com ponderação T1, o miocárdio que sofreu enfarcte irá apresentar elevada intensidade de sinal (tom claro na imagem) comparando com baixa intensidade de sinal (tom escuro na imagem) do miocárdio saudável.

De forma a auxiliar a distinção de sinal entre os dois tecidos, uma sequência de gradientes IR é geralmente utilizada.

Uma sequência IR consiste na aplicação de um impulso de radiofrequência de 180º despoletado por cada onda R na leitura electrocardiográfica (ECG) do paciente. Inicialmente, a magnetização longitudinal (Mz) possui um valor inicial denominado M_{z0}. Com a aplicação do impulso de inversão, o vector soma Mz é rodado em 180º convertendo M_{z0} em $-M_{z0}$. Após o impulso de inversão, a magnetização longitudinal irá então recuperar de $-M_{z0}$ a M_{z0}. O tempo de inversão (TI) caracteriza o período de tempo entre a aplicação do impulso de inversão e o momento de aquisição. O TI é selecionado de forma a coincidir com o ponto nulo de determinado tecido (usualmente o miocárdio saudável) permitindo anular o sinal desse mesmo tecido.

Resumindo, enquanto que por um lado a distribuição diferenciada do agente de contraste permite aumentar a intensidade de sinal do miocárdio que sofreu enfarte, a aplicação da sequência IR permite anular o sinal do miocárdio saudável. A junção de

ambos leva à obtenção do melhor contraste de sinal entre os dois tecidos.

Uma vez que DE-MRI desempenha um important papel na avaliação de doenças cardíacas, a procura por uma melhoria na qualidade de imagem e ausência de artefactos, tem impulsionado vários projectos de investigação nos últimos anos. Algumas limitações inerentes à técnica ainda permanecem por solucionar.

Tratando-se de uma técnica *cardiac triggered*, irregulariedades no batimento cardíaco influenciam directamente o comportamento da magnetização longitudinal e consequente sinal adquirido. Esta irregulariedade do sinal adquirido leva ao aparecimento de artefactos na imagem final quando reconstruída.

Este projecto consistiu em avaliar de que forma irregulariedades no batimento cardíaco influenciam o sinal adquirido e consequente aparecimento de artefactos na imagem final. Assim como posterior desenvolvimento e teste de um novo método de redução de artefactos das imagens em pacientes com um batimento cardíaco irregular.

Diversos métodos de redução de artefactos através da otimização do TI têm sido apresentados na comunidade científica. Estes pretendem diminuir a dispersão do sinal do miocárdio saudável através de otimização do TI para cada intervalo cardíaco. No entanto, a otimização do TI é dependente de T1 e a minimização de variações do sinal do miocárdio saudável pode gerar artefactos devido ao sinal proveniente dos restantes tecidos que não foram corrigidos. O método de correção sugerido nesta dissertação procura eliminar esse factor e otimizar dinamicamente o TI tendo em conta simultaneamente o sinal de vários tecidos.

O projecto consistiu primeiramente na construção de um ambiente de simulação numérica e posterior implementação em scanner clínico 3T utilizando fantomas experimentais.

O ambiente de simulação encontra-se dividido em várias funções modulares. Uma primeira função permite obter um registo simulado de ECG, representando o nosso paciente virtual, podendo simular diferentes intervalos de tempo entre picos R com um determinado desvio-padrão (10%,20%...etc.) da média de batimento cardíaco.

De seguida, uma segunda função calcula a intensidade de sinal ao longo de cada janela de aquisição tendo em consideração diversos parâmetros iniciais. Sendo os principais: TI, TR (tempo de repetição), TE (tempo de eco), o sinal de ECG e o factor de aquisição. O

factor de aquisição (N) permite definir o número de pontos do espaço-K adquiridos por cada janela de aquisição.

Uma terceira função modular simula a aquisição de imagens 2D utilizando como *input*: um fantoma virtual, a intensidade de sinal previamente calculada e uma trajectória de aquisição no espaço-K. O fantoma virtual utilizado pretende representar um corte de curto eixo do ventrículo esquerdo com três tecidos presentes: miocárdio que sofreu enfarte, massa de sangue no interior do ventrículo e miocárdio saudável. De seguida, cada ponto de intensidade do sinal de cada vez pré-calculado através do T1 do tecido correspondente é atribuido à máscara do tecido correspondente no fantoma virtual. Após soma das três máscaras de intensidade (três tecidos)e aplicação de uma transformada de Fourier (FFT), o espaço-K final é obtido. Posteriormente, a trajectória de aquisição do espaço-K é utilizada de forma a re-organizar a ordem em que este é preenchido. Por último, após transformação do espaço K através de uma transformada inversa de Fourier (IFFT) (do inglês *Inverse Fast Fourier Transform*), obtém-se a imagem final reconstruida.

A quarta função modular aplica o método de correção de artefactos por otimização do TI. O principal objectivo consiste em determinar o TI ótimo (TI_{opt}) que corresponde à minimização de variações do sinal (SSE_{total}) dos vários tecidos considerados: $SSE_{total} = W * SSE_{myocardium} + (1 - W) * SSE_{blood}$. Onde W é o factor que permite contra-balançar a correção dando mais ponderação a artefactos originários do sangue (W<0.5) ou do miocárdio saudável (W>0.5).

Por último, o método proposto foi implementado em scanner clínico Philips 3T utilizando fantomas de gel de forma a representar os três tipos de tecidos (miocárdio que sofreu enfarte, sangue e miocárdio saudável). Para aquisição dos dados em scanner, os mesmos parâmetros de aquisição e sinal de ECG previamente calculados no ambiente de simulação, foram utilizados.

Resultados obtidos com a simulação numérica confirmaram que um batimento cardíaco irregular afecta directamente o comportamento do sinal adquirido. Por exemplo para 50% de variação do batimento cardíaco, o sinal do miocárdio saudável apresentou mais de 85% de dispersão em relação ao valor médio enquanto que o sangue revelou quase 30% de desvio. Verificou-se também que irregulariedades do batimento cardíaco levam a maiores desvios de intensidade do sinal do miocárdio saudável e do sangue. Para além

disso, a simulação de imagens 2D revelou o aparecimento de artefactos com intensidade crescente de acordo com a intensidade de variação do batimento cardíaco.

Implementação do método de otimização do TI foi executada com sucesso e revelou resultados positivos. Medições do nível geral de artefactos da imagem simulada para diferentes valores de W, permitiram concluir que o valor ótimo de W corresponde a 0,4.

Para uma situação de 50% de variação do batimento cardíaco e utilizando o método de correção com W=0,4, verificou-se uma diminuição na variação do sinal do miocárdio saudável de 90 % para aproximadamente 25% e no sinal do sangue de 20% para menos de 10%. Tal como esperado, uma redução na variação de intensidade do sinal reflectiu-se na diminuição da quantidade de artefactos na imagem final. Assim, verificou-se uma redução de 70% dos artefactos comparando com uma imagem não corrigida. Correspondendo 20 e 30 % mais comparando com corrigir apenas um tecido de cada vez, sangue e miocárdio saudável respectivamente.

Resultados similares foram obtidos nos dados experimentais adquiridos no scanner, com similar redução do nível de artefactos na imagem final. Medição do nível de artefactos nas imagens 2D dos fantomas experimentais levaram à conclusão que o método permitiu reduzir ainda mais o nível de artefactos comparando com os dados simulados. Com o método de otimização do TI a W=0.4, a imagem apresentou uma redução de mais de 40% comparando com uma correção de apenas o miocárdio saudável.

Resumindo, os resultados experimentais foram coincidentes com os resultados simulados e parecem suportar a conclusão que a otimização do TI tendo em conta múltiplos tecidos reduz com sucesso a quantidade de artefactos em imagens DE. No entanto, o estudo apresenta algumas limitações. Os valores de T1 dos fantomas experimentais foram determinados através de uma sequência Look-Locker. No entanto, alguns resultados obtidos sugeriram que a errada estimação dos valores de T1 poderá ter ocorrido, o que levou ao desvio nos resultados obtidos.

Aspectos como variar a média do batimento cardíaco para valores inferiores ou superiores, teste diferentes trajectórias de aquisição do espaço-K, novo teste dos valores de T1 dos fantomas, assim como determinação dos parâmetros de aquisição para imagens *in-vivo* são importantes aspectos a considerar em estudos futuros.

Em conclusão, este estudo contribuiu positivamente para um conhecimento mais

alargado em termos da diminuição de artefactos imagens DE-MRI. Concluiu-se que uma abordagem à otimização de TI onde múltiplos tecidos são considerados apresenta vantagens relativamente à abordagem em que apenas a contribuição do miocárdio saudável é tida em conta.

Palavras-chave: DE-MRI (Delayed enhancement Magnetic Resonance Imaging), Tempo de inversão (TI), Enfarcte do miocárdio, Batimento cardíaco irregular

Abstract

Delayed Enhancement Magnetic Resonance Imaging (DE-MRI) is a widely used imaging tool in the assessment of ischemic pathologies, crucial in distinguishing between infarcted and healthy myocardium [1]. Usually, T1 weighted images are acquired using an Electrocardiogram (ECG) triggered Inversion Recovery (IR) sequence after contrast agent injection which allows to increase signal contrast between the two tissues.

Since DE-MRI is cardiac triggered, heart rate (HR) irregularities directly affect signal behaviour. When HR varies, the time for the longitudinal magnetization (Mz) to recover is different for each cycle which leads to a different amount of magnetization available for acquisition. This irregular signal intensity can cause strong image artefacts.

Therefore, the purpose of this study was to develop a novel acquisition approach to compensate for HR variations using a multi-tissue model. Optimal Inversion Time (TI) values for each cycle were obtained by minimizing Mz variations of the healthy myocardium ($SSE_{myocardium}$) and blood (SSE_{blood}): $SSE_{total} = W * SSE_{myocardium} + (1-W) * SSE_{blood}$. The weighting (W) allows to correct more strongly for artefacts from blood (W < 0.5) or myocardium (W>0.5) to achieve the best image quality possible.

Simulations were performed to study signal behaviour and test the proposed multi-tissue correction approach. In addition, the method was also implemented on a 3T scanner and phantom experiments verified the simulated results.

The proposed multi-tissue method was successful when compensating for artefacts. For 30% HR variation scenario, it reduced image artefacts by approximately 70 % compared with a non-corrected image which is 20 and 45 % more than the single-tissue approach, only blood or healthy myocardium respectively.

In conclusion, not only the proposed multi-tissue method can be successfully used to reduce image artefacts, but also leads to a better image quality than some previously

presented approaches with a single tissue correction.

Keywords: DE-MRI, ischemic heart disease, inversion time (TI), irregular heart rate, arrhythmia

Acknowledgements

Although only one name appears at the front page, writing this dissertation would have been impossible without the crucial contribution from several people.

Firstly, many thanks to my supervisor Professor Rita Nunes for point out the way from the beginning, never forgetting some encouraging words when I was feeling lost.

I'm also extremely grateful to my external supervisor Professor Tobias Schaeffter, whose expertise carried this project to successful grounds and for the opportunity granted to work within such an amazing research group.

I would like to express my deepest gratitude to Dr. Christoph Kolbitsch for his patient, knowledge and perseverance even in the hardest hours of the project. From whom I learned that it is possible (or perhaps essential) to have passion for the work we do.

I would also like to thank to all the department staff for receiving me so nicely and making me feel part of the team. Many thanks to everyone in the *cake club* for their companionship and for making me leave King's College London (KCL) not only with deep knowledge in medical imaging but also in baking!

I gratefully acknowledge financial support from the Eramus student interchange Grant.

This dissertation is much more than one single project, it is the end of a journey that started almost 5 years ago. To all my colleagues (*aka* second family) at FCUL many thanks for all the fun moments. Thank you Catarina for the friendship and travelling along with me the same hard road. Thank you Carla for all the fun moments in London. Thank you Mariana for some (very!) important discussions about make up and croissants.

Many thanks to my friends "Mutantes" just for being there in the last few (ok...many, many) years.

And thank you Luis, who keeps having to explain everyone that I take "heart pictures"

(which is actually true!) but nevertheless was a major source of unconditional support.

Finalmente mas nunca em último, esta tese é dedicada aos meus pais e irmã. Que sempre me ensinaram que o conhecimento não ocupa lugar.

Um grande obrigada a todos!

Contents

List of Figures

List of Tables

List of Abbreviations

CAD Coronary artery disease.

DE-MRI Delayed Enhancement Magnetic Resonance Imaging.

DTPA Diethylene-Triamine-Penta-acid.

ECG Electrocardiogram.

FCUL Faculty of Science, University of Lisbon.

Gd Gadolinium.

IBEB Institute of Biomedical Engineering and Biophysics.

IR Inversion Recovery.

KCL King's College London.

MI Myocardium infarction.

RF Radio Frequency.

SPECT Single photon emission tomography.

SSE Sum of Squared Error.

TI Inversion Time.

UK United Kingdom.

Chapter 1

Introduction

The present dissertation describes the project developed by the author to complete an Integrated Master degree in Biomedical Engineering and Biophysics - Radiation in Diagnosis and Therapy profile, at Faculdade de Ciências, Universidade de Lisboa (FCUL), Portugal.

The project was developed at the Division of Imaging Sciences and Biomedical Engineering, KCL, United Kingdom (UK). This was under the LLP/Erasmus student interchange program for a period of eight months between October 2012 and May 2013.

During this project a novel approach to reduce artefacts due to heart rate variations in DE-MRI was developed.

Professor Tobias Schaeffter, deputy head of the Division of Imaging Sciences and Biomedical Engineering, with extensive experience in imaging sciences was the external supervisor. Close collaboration with Dr. Christoph Kolbitsch, post-doctoral associate at the department, was also crucial for the project accomplishment.

Professor Rita Nunes, post-doctoral researcher at the Instituto de Biofísica e Engenharia Biomédica (IBEB), FCUL and assistant teacher at FCUL was the internal supervisor. Professor Nunes works mainly at IBEB but also has current projects at KCL, allowing to establish the contact between the two research groups.

1.1 Project background

Since the 1980s MRI has been used to assess myocardial infarction with the use of contrast agents [2]. Commonly, T1 weighted images are obtained using a cardiac triggered IR gradient echo sequence after contrast agent injection [3–5].

This leads to a high signal contrast and consequent distinction between the myocardium that has suffered irreversible infarction (necrotic tissue) and the healthy myocardium, being a useful tool for physicians to evaluate the extent of non-viable myocardium and therapeutic course in a wide set of cardiac pathologies.

Any cardiac MRI technique is challenging due to the cardiac and respiratory chest motion. This can be usually compensated for with cardiac triggering, where data is acquired in the period where the heart is more steady (mid-diastole), and breath hold or respiratory navigators [6].

However, patients with irregular heart rates still pose a major challenge for DE-MRI. Since it is cardiac triggered technique, irregular heart rate can directly influence the acquired MR signal. When the heat rate varies, the time for the longitudinal magnetization to recover is different for each cardiac cycle which leads to a different amount of magnetization available at the time of data acquisition. This irregular magnetization behaviour leads to a variation of the acquired signal, causing strong artefacts when the final image is reconstructed [7].

As DE-MRI becomes a widely used cardiac imaging tool, the demand for high quality images increases proportionally and several studies have been presented to compensate for this limitation in the past few years [8–10].

Most methods compensate for this limitation by adapting the TI for each cardiac cycle to ensure the healthy myocardium signal is always nulled [8, 9]. Nevertheless this TI correction is T1 dependent and correcting for the healthy myocardium can create artefacts arising from other tissue types, such as from the blood pool.

The overall goal of the project was to develop a method to reduce artefacts due to arrhythmia considering a multi-tissue approach. The main goal is to correct the TI such that the magnetization available at acquisition remains as stable as possible. A more stable magnetization behaviour will translate in a final image with fewer and less

pronounced artefacts.

Firstly, a numerical simulation was built to study signal behaviour under the influence of irregular HR and develop the novel correction method. Secondly, the correction method was implemented at a 3T scanner using the same parameters. Experimental data from gel phantoms was used to validate simulated results.

1.2 Thesis outline

This thesis is divided into 5 chapters. Chapter 1 is the current chapter. A brief resume of the project background, respective supervisors and development is given.

Chapter 2 presents a background introduction to important concepts of DE-MRI. Technical aspects of the technique are explained such as medical applications, functioning of an IR sequence acquisition, choice of the TI and main limitations of DE-MR images. In addition, a brief explanation of current image artefacts correction methods is also given.

Chapter 3 refers to the first portion of this dissertation study, the built of a numerical simulation environment. Methodology referring to the construction of the simulation environment as structure, main functions, mathematical description of the signal and parameters used, can be found in this chapter. In addition, the simulated results are also presented.

Chapter 4 presents the second portion of the study: phantom experiments in a 3T scanner. Both the methodology and results referring to the scanner experiments are shown.

Chapter 5 is a summary of this dissertation, including the conclusions drawn from the study, its contribution for the scientific community, main limitations and recommendations for future studies in the field.

Chapter 2

Delayed Enhancement MRI: theoretical background

2.1 Introductory considerations

In DE-MRI, T1 weighted images are usually obtained using a cardiac triggered IR sequence acquisition after contrast injection. DE imaging is most commonly used for discrimination between healthy myocardium and infarcted myocardium, for medical diagnosis and therapeutic establishment purposes [1, 11].

As the name indicates, delayed enhancement imaging distinguishes itself from enhancement imaging by delaying the acquisition by a certain period of time (usually between 10 to 20 minutes) after contrast injection [12]. Therefore this technique allows to differentiate the tissues based on their distinct wash-out times [1]. A slower wash-out rate directly relates to a larger concentration of the contrast agent left in the tissue when acquisition is performed. Since the most commonly used contrast agents cause a shortening effect of the T1 relaxation time, tissues with a higher concentration of the agent will present a shorter T1 value and thus a higher signal intensity in the final image.

In addition, a proper adjustment of the IR pulse sequence (i.e. selecting the inversion time such that the obtained signal from the healthy myocardium is null) increases the signal contrast between the healthy and infarcted myocardium.

The next sections of this chapter explore in depth these two main aspects of DE

imaging, as well as medical applications and limitations underlying this technique.

2.2 Ischemic heart disease and DE imaging medical applications

Ischemic heart disease is the leading cause of death in adults in the world. In 2011 alone, approximately 7 million people died from ischemic heart disease [13].

Ischemic heart disease (or Myocardium infarction (MI)) is a heart pathology characterized by the malfunction of the heart wall due to partial or complete obstruction of the blood supply (ischemia). Ischemia causes a shortage of oxygen and vital nutrients to the correct functioning of the heart muscle.

In most patients, ischemic heart disease is related to another pathology called Coronary artery disease (CAD). CAD is characterized by the formation of an atherosclerosis plaque (substance made of cholesterol, fat and blood compounds) [14] which can lead to the hardening and narrowing of the coronary arteries [15]. The two coronary arteries (left and right) are responsible for irrigating the heart muscle. CAD and consequent malfunction of those arteries lead to heart muscle ischemia.

The myocardium can be affected to several degrees, from infarcted myocaridum (necrotic tissue) to hibernated myocardium. While hibernated myocardium presents minimum contractile function due to restricted blood supply but can recover after vascularization therapy, infarcted myocardium presents permanent cell destruction [16].

Additionally in clinical terms, distinction between acute and chronic MI is considered. Acute MI is usually characterized by necrotic cells (ruptured cellular membrane) and an enlarged extracellular volume. On the other hand, in chronic MI the absence of cells for a prolonged period led to the formation of a collagen matrix (fibrotic tissue) [1, 15]. Representation of both MI types and an healthy myocardium can be seen in Fig. 2.1.

Currently, Single photon emission tomography (SPECT) is one of the most common techniques used when assessing MI, since it can directly indicate metabolic function of the myocardium cells [17]. Nevertheless, it yields low spatial resolution images and does not provide high detailed information. MRI not only presents higher spatial resolution, it

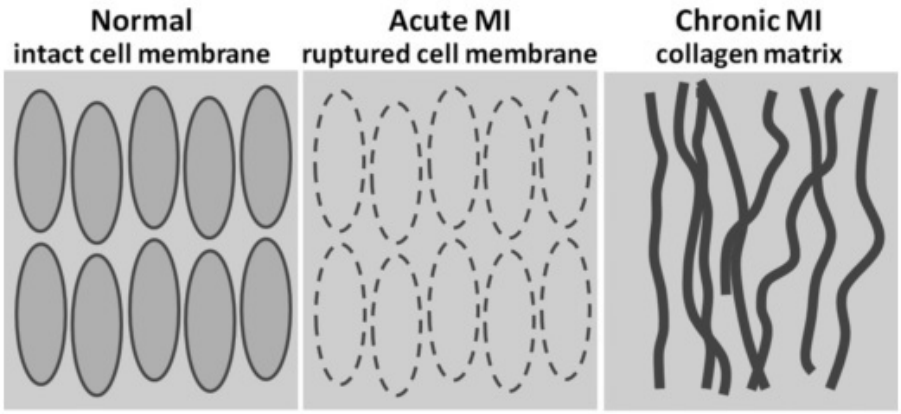

Figure 2.1: Representation of a healthy myocardium with intact cells, acute MI with ruptured cell membranes leading to cellular death and chronic MI with formation of fibrotic tissue. (Image modified from [1])

also leads to higher reliability for some types of MI that are undetectable with SPECT. In a study by Wagner et al, MRI was reported to correctly identify 92% of sub-endocardial infarction segments while SPECT was only able to identify 30% [18].

Due to a higher spatial resolution, absence of ionizing radiation and multiplicity of applications, DE-MRI has become a well accepted alternative for cardiac diagnosis.

When dealing with MI patients, assessment of myocardium viability is crucial for predicting heart function recovery chance, deciding on a therapy course and calculating patient re-incidence rate. Assessment of myocardium viability consists in distinguishing between hibernated myocardium and infarcted myocardium.

In DE imaging, infarcted tissue usually presents enhancement after contrast injection while hibernated myocardium does not. Previous studies proved that tissue showing enhancement (infarcted myocardium) continue to show lack of contraction even after vascularization therapy [19,20]. Thus supporting the theory *"bright is dead"* where enhanced tissue is most likely irreversibly damaged [21]. In summary, enhancement in a certain portion of the heart wall in DE imaging is most likely related with infarcted myocardium.

High reliability of MRI when matching infarct size to histology measurements (Fig. 2.2) was shown by Wagner et al. A high correlation coefficient (R=0.98) was reported between infarction size assessed with DE-MRI and assessed with histology measurements

[18].

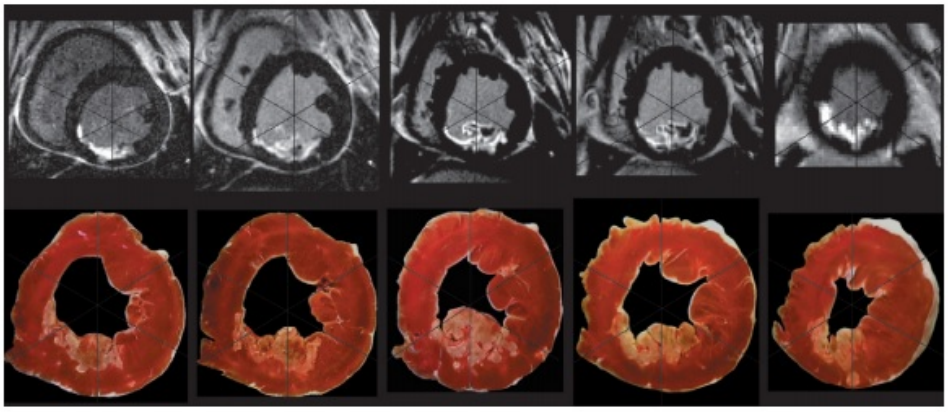

Figure 2.2: (Top) Short axis view of the heart obtained with DE-MRI showing enhanced myocardium infarction. (Down) Correspondent histological slices with correspondent MI areas [18].

Another positive aspect of DE-MRI is that both acute and chronic MI show enhancement (Fig. 2.3). Nevertheless, some disagreement is still present regarding whether DE-MRI can be useful in distinguishing between the two of them. One current suggestion refers to using the presence of oedema (tissue swelling due to water accumulation) as the differentiating factor since it is only present in acute MI. Since water usually presents a long T1 and T2 values comparing with healthy myocardium, signal contrast arises between the oedema (acute MI) and the healthy myocardium. Current studies reported good results when identifying oedema in acute MI [22, 23]. This is accomplished by using a technique that uses both DE imaging and T2 weighted images.

DE-MRI can also be used to predict muscle function recovery after therapy. Previous studies presented evaluation of transmural extent of infarction area as a way to predict contractile improvement after therapy [24, 25]. For example, Choi et al. study concluded that when the percentage of tissue that showed improvement was reduced, the transmural enhanced infarction area increased. For segments with 1 to 20% infarction extent, around 67% showed contractible improvement but for 76% infarction extent in DE imaging, only 5% showed function improvement [24].

This conclusions can be useful when assessing a patient course of therapy and chance of contractile recovery even before therapy is applied.

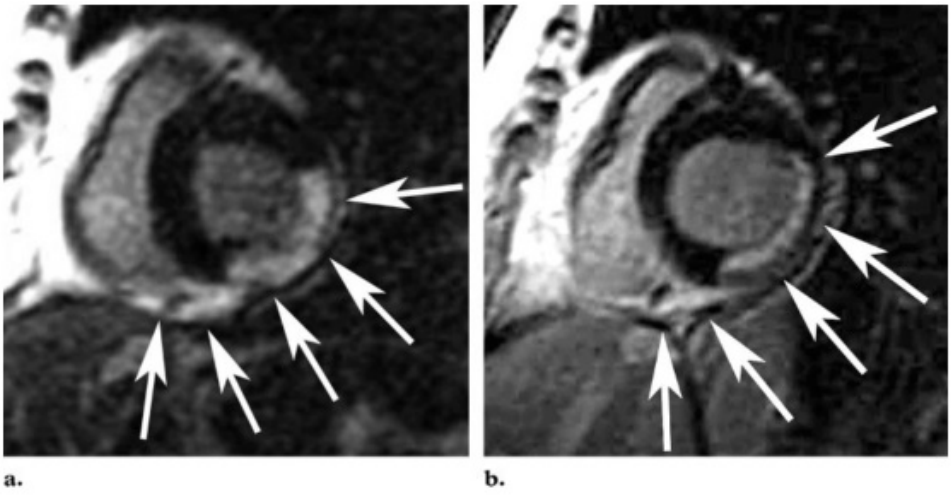

Figure 2.3: (a) Short axis DE-MRI view of the heart showing acute transmural MI. Enhancement of the infarcted myocardium is visible (arrows) compared to a null signal from the healthy myocardium (dark tone). (b) Short axis DE-MRI view of the hear from the same patient one year later (chronic MI). Infarcted myocardium continues to show enhancement and also shows thinning of the infarcted area compared to the acute MI phase [16].

DE might also be useful in patients with no previous history of myocardium infarction episodes but diagnosed CAD. It was reported that 81% of the patients with CAD, diagnosed by X-ray angiography, showed delayed enhancement compared to only 8% in the control group. Therefore, DE might be a valid alternative to ionizing radiation methods when evaluating CAD patients and preventing future heart failure episodes [17].

While assessment of ischemic heart diseases is the most common usage for DE imaging, it is not exclusive and can be seen in a wide range of cardiac pathologies. A few examples are inflammatory diseases of the myocardium, cardiac neoplasms or genetic conditions [16].

2.3 Physiologic basis and contrast agent behaviour

Myocardium infarction assessment using DE imaging relies on different wash-out rates of the contrast agent and consequent effects on T1 values of the cardiac tissues.

The majority of contrast agents work by altering the T1 and T2 relaxation times of the surrounding tissues. According to the model described by Bloembergen, Purcell and

Pound [26], the effect of contrast agents on T1 and T2 relaxation times can be described by:

$$\frac{1}{T1} = \frac{1}{T_{1,0}} + R_1 n_a \tag{2.1}$$

$$\frac{1}{T2} = \frac{1}{T_{2,0}} + R_2 n_a \tag{2.2}$$

Where T1 and T2 are the relaxation times with contrast agent influence, $T_{1,0}$ and $T_{2,0}$ are the relaxation times in the absence of contrast agent, n_a is the agent's concentration and R_1 and R_2 are the agent's relaxivity values. Relaxivity quantifies the ability of a certain compound to change the relaxation rates of the surrounding proton spins per molar concentration.

The most commonly used agent in DE-MRI is a Gadolinium (Gd) based compound called DTPA-Gd. The gadolinium atom has seven unpaired electrons, giving it strong paramagnetic properties and becoming strongly magnetized when placed in an external magnetic field. Nevertheless, Gd is highly toxic in it's pure state, being necessary to chelate it with another compound called Diethylene-Triamine-Penta-acid (DTPA). Thus making Gd thermodynamically more stable and biologically safer [27].

Gadolinium based agents comply to Equations 2.1 and 2.2 and present high values of relaxivity thereby shortening T1 and T2 times of surrounding tissues.

Distinct distribution of the agent in DE-MRI depends not only on the Gd kinetics but also on physiological characteristics of the heart tissues involved. Due to the chelation with DTPA, Gd presents a large molecular weight, having tendency to accumulate in tissues with larger extracellular volume [15]. Since tissues that suffered infarction usually present an enlarged extracellular space (Section 2.2), they tend to accumulate higher amounts of the contrast agent.

In addition, the delay period between contrast injection and acquisition ensures that most of the contrast agent has already washed out from the healthy tissue but remains in higher concentration in MI tissues.

In conclusion, tissues with higher Gd concentration (infarcted tissue) have a shorter T1 value and consequently appear bright on T1-weighted images. On the other hand,

tissues with longer T1 values (less Gd concentration) appear darker, such as the healthy myocardium. The blood pool tends to present an intermediate T1 value.

2.4 Inversion recovery pulse sequence and inversion time

Distinct distribution of the contrast agent between the different heart tissues allows for the infarcted myocardium to be slightly more enhanced than the healthy tissue. In addition, an IR pulse sequence is usually used to achieve the best signal contrast possible between the two tissue types [28].

Inversion recovery is a gradient echo pulse sequence where a 180º pulse precedes a gradient echo read-out. However, 2D MR images relate to a large amount of data and image acquisition has to be divided into several sections (over several acquisition windows). In addition, the acquisition window length is limited by mid-diastole, thus a limit number of K-space lines can be sampled per cardiac cycle. Thereby the read-out portion is repeated N times to allow acquisition of multiple data points per inversion pulse (Fig. 2.4) [15].

Initially, the magnitude of the net vector of longitudinal magnetization is positive and described as Mz_0. Application of the inversion pulse flips the magnetization vector by 180º transforming Mz_0 into $-Mz_0$. After the IR pulse, longitudinal relaxation occurs [15]:

$$M_z(t) = M_{z,eq}(1 - 2e^{-\frac{t}{T1}}) \tag{2.3}$$

Where T1 is the longitudinal relaxation parameter and $M_{z,eq}$ the magnetization at equilibrium. Longitudinal relaxation curves (Equation 2.3), without considering read-out, for healthy and infarcted myocardium can be seen in Fig. 2.5.

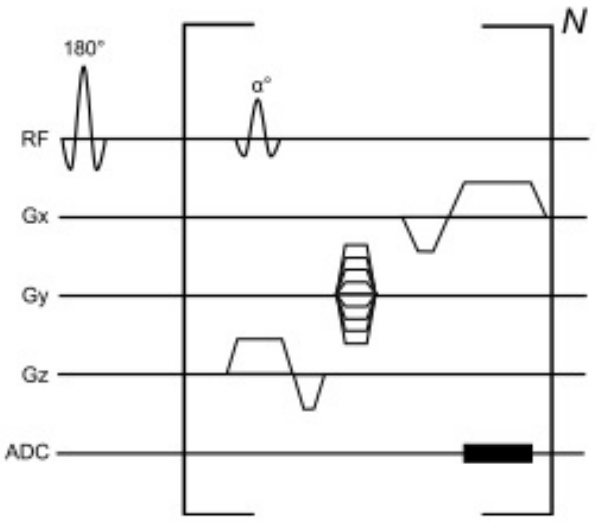

Figure 2.4: Inversion recovery gradient echo sequence diagram. Firstly an 180° Radio Frequency (RF) pulse is applied to cause inversion of the net Mz vector, followed by a gradient echo read-out (inside brackets). The brackets portion can be applied several times per cardiac cycle to allow the acquisition of multiple segments within the same inversion pulse. The excitation RF pulse is applied, flipping the available longitudinal magnetization towards the xy-plane by the angle defined by α. Secondly, the echo is obtained through application of a bipolar frequency-encoding gradient (Gx). Firstly to dephase the protons spins and the secondly as frequency read-out. Gy gradient defines the phase-encoding gradient that allows to define the K-space line that it is being sampled. The Gz gradient is the slice selection gradient allowing to select the 2D slice. Finally, the ADC (analogue to digital converter) allows for the signal to be acquired [15].

The time point where the magnetization is zero (null point) depends on T1 and can be used to null the signal from a chosen tissue. The time period between the inversion pulse and excitation is the TI. This is usually selected such that the healthy myocardium signal is null, relating to the best signal contrast between healthy and infarcted myocardium [1].

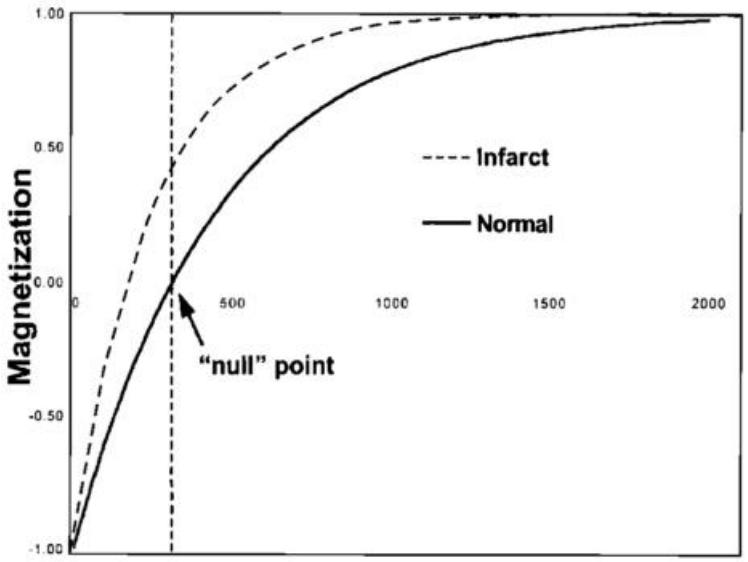

Figure 2.5: Longitudinal magnetization relaxation curves for healthy myocardium (longer T1) and infarcted myocardium (shorter T1) after application of an IR pulse. The "null point" corresponds to the time point for which the healthy myocardium signal is null [2].

2.4.1 Selecting the time of inversion

Selecting the appropriate TI is a crucial step to obtain a good image quality and a diminished level of artefacts.

Nevertheless, several drawbacks can be encountered. Firstly, the TI varies from patient to patient and so it is empirically determined for each subject [29]. Secondly, it also depends on several factors such as: contrast agent administrated dose, cardiac function, time after contrast injection, among others [28].

Mathematically it is possible to determine the appropriate TI from its dependency of the T1 of the healthy myocardium. Following from Equation 2.3, the tissue signal is null when $M_z(TI_{null}) = 0$, therefore TI can be estimated:

$$M_z(TI_{null}) = M_{z,eq}(1 - 2e^{-\frac{TI_{null}}{T1}}) = 0 \tag{2.4}$$

$$TI_{null} = -T1ln(2) \tag{2.5}$$

However, in *in-vivo* situations, it is not possible to know the accurate value of T1 of the myocardium *a priori*.

Several methods are presented throughout the literature to determine the optimal TI, for example, using cine MR scout images or T1 mapping measurements [28, 30].

Using cine IR images to estimate TI is a trial and error technique. After the usual 180º IR pulse is applied, a fast steady-state free precession readout is implemented allowing to acquire multiple images along the longitudinal recovery curve, correspondent to different TI values (Fig. 2.10). The optimal TI corresponds to the visually selected image where the healthy myocardium appears to have a null signal [28].

As an alternative, the TI can be estimated through direct T1 mapping measurements [15, 30] using a Look-Locker sequence [31]. This allows to more accurately estimate T1 of the healthy myocardium and correspondent adequate TI (Equation 2.5).

The incorrect selection of the inversion time can lead to image artefacts and mislead during evaluation of the myocardial infarction (Section 2.5).

2.4.2 Imaging time after contrast agent injection

As equally important as the selecting the correct TI, choosing the imaging time after contrast injection is another major concern in DE-MRI.

Each tissue signal intensity directly depends on the present Gd concentration level within the tissue at the time of acquisition (Section 2.3). However, Gd concentration doesn't remain steady and gradually washes out with imaging time. Thereby, the chosen TI might no longer be adequate and needs to be adjusted if acquisition takes too long [2].

Figure 2.6 shows the direct relation between Gd concentration and the TI value. Exponential decrease of plasma Gd concentration with time (solid line) is based on real data acquired by Weinmann et al for a Gd injection dose of 0,125 mmol/Kg [32]. The dashed line describes the correct TI necessary to null the myocardium calculated from Gd concentration at a given time [33]. For example, at 5 minutes after injection, the correct TI is estimated to be approximately 304 ms.

The idea to keep in mind is that diminished Gd concentration translates to a weaker T1 shortening effect resulting in tissue with a longer T1 and consequent need to increase the TI [33]. Correct estimation of the TI might be possible but it is important to consider that it is transient for each cardiac cycle and if acquisition takes too long, it might no

longer be nulling the myocardium signal for the last data points acquired.

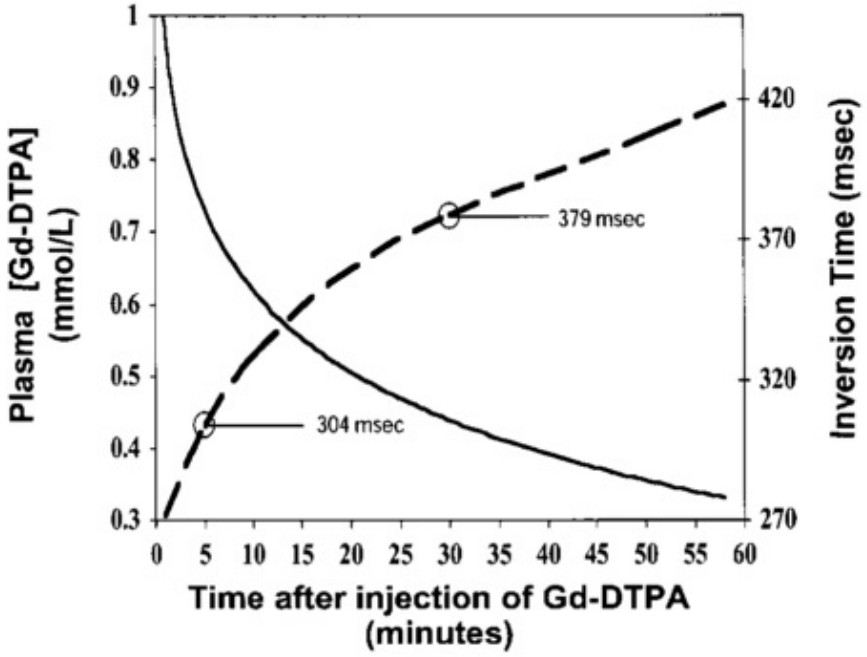

Figure 2.6: Concentration of Gd plasma as a function of time after injection (solid line) and appropriate TI for correspondent Gd concentration (dash line). As imaging time after injection increases, the adequate TI for a certain dose of Gd also increases [2].

In addition, another study suggested that imaging time after contrast injection can also affect infarct size estimation. Oshinki et al suggested that for a Gd dose of 0,03 mmol/kg, data should be acquired at 21 $\pm$ 4 minutes after injection so that the enhanced area matches true MI size. On the other hand, images acquired right after injection (within the 10 minutes range) overestimated infarcted size by 20-40 % [34].

In conclusion, both studies seem to suggest that imaging time after injection plays a crucial role in ensuring correct signal nulling of the myocardium.

2.4.3 Repeated IR time sequence and triggering

A repeated IR sequence is usually applied to allow acquisition of a segmented 2D image matrix over several acquisition cycles.

A schematic representation of a repeated IR acquisition is shown in Fig. 2.7.

Each IR pulse is triggered by an R-peak on the ECG signal. However, a delay period

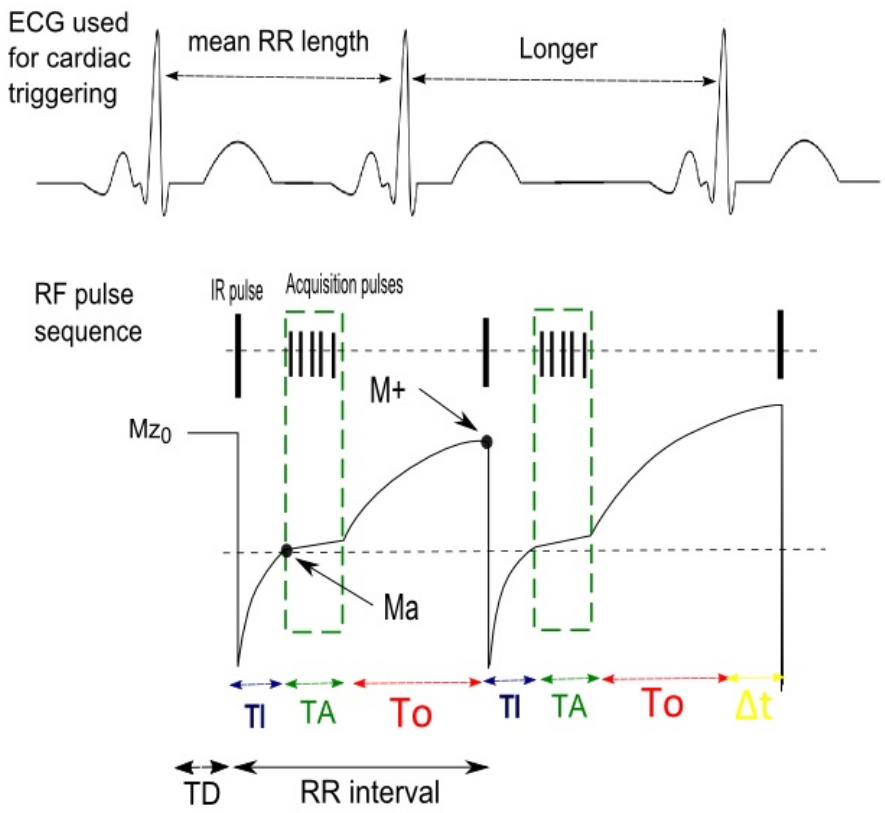

Figure 2.7: Schematic representation of longitudinal magnetization from the healthy myocardium along a repeated IR sequence. The first cycle represents a steady HR (mean R-R length) while the second cycle represents an irregular HR situation (longer interval than mean R-R).

(TD) introduced between the R-peak triggering and inversion pulse application, allows for acquisition to occur in mid-diastole. After the IR pulse, $-Mz_0$ is allowed to recover until Ma (Mz available at acquisition) when the read-out sequence portion is applied. The TI is selected such that acquisition begins at the time point for which the healthy myocardium signal is null. The MR signal can then be acquired by flipping Ma towards the xy-plane (Mxy). During acquisition (dashed box), several consecutive acquisition pulses (α), equidistant by a time period TR, are applied to acquire multiple data points. Acquisition is set to last for a time period TA. Finally, the last Mxy point is allowed to recover until M_+ (Mz available before the next inversion) for a period of time T0.

If the heart rate is steady (mean R-R length), the following equation is found:

$$RR = TI + TA + T_0 \tag{2.6}$$

If the heart beat is irregular, an extra Δt can either be positive (R-R interval is longer than mean R-R) or negative (R-R interval is shorter than the mean):

$$RR = TI + TA + T_0 \pm \Delta t \tag{2.7}$$

In terms of triggering, DE imaging can use R-R or 2R-R (Fig. 2.8). This means that the IR pulse can either be applied for every R peak occurrence (R-R) or for every other R peak (2 R-R). Using a R-R gating reduces the amount of time available between IR pulses which leading to incomplete magnetization recovery. On the contrary, a 2R-R gating allows for a more complete magnetization recovery and is specially recommended for tachycardia patients. However, 2 R-R gating does require twice the acquisition time [1].

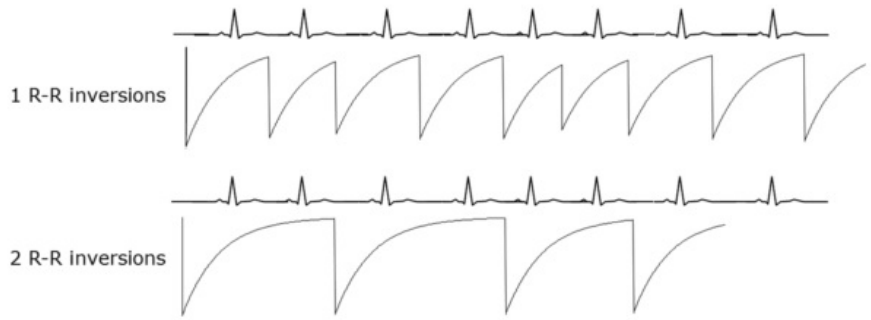

Figure 2.8: (Top) Mz behaviour when R-R gating is used leading to incomplete magnetization recovery. (Bottom) Mz behaviour when 2R-R gating is considered, improving magnetization recovery and allowing to obtain higher signal intensity [1].

2.5 Image artefacts and limitations

A major concern in DE-MRI, as in any cardiac imaging modality, is the presence of image artefacts due to cardiac motion.

For DE-MRI restricting data acquisition to a so-called acquisition window placed during the mid-diastolic period is usually a successful compensation technique [6]. However,

not only there is cardiac motion but respiratory motion of the chest as well. The latter is usually compensated for by breath-holding or respiratory navigation approaches.

Nevertheless when those are deficient, specific artefacts can be identified. Deficient breath holding usually causes ghosting of chest area while poor cardiac gating causes ghosting of the heart itself (Fig. 2.9).

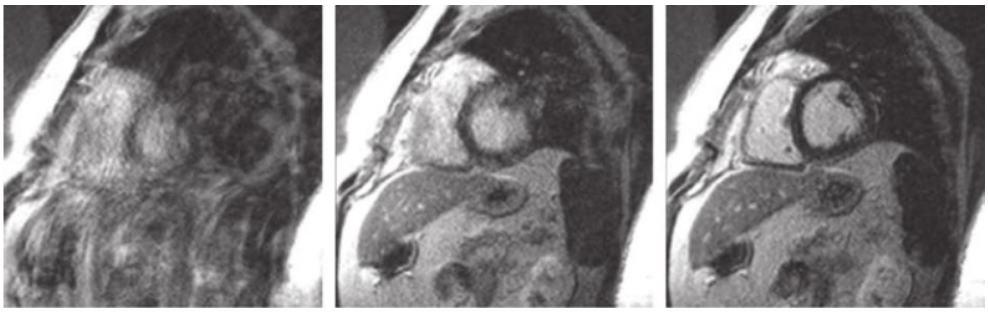

Figure 2.9: Image DE-MRI showing: (a) ghosting artefacts of the overall chest area due to deficient breath holding (b) ghosting artefacts of the heart itself due to poor cardiac gating (c) no ghosting artefacts due to acquisition with correct breath hold and gating [6].

When imaging tachycardia patients, it is crucial to use 2R-R or even 3R-R gating to allow for complete magnetization recovery. That will ensure higher signal intensity and less ghosting artefacts [1].

Patients with tachycardia also present another challenge to DE imaging since their mid-diastole period is usually shorter. To reduce ghosting due to heart movement, the acquisition window duration has to be shortened with less K-space lines sampled per window [6].

Another source of inaccurate images can be the incorrect choice of TI (Fig. 2.10).

When the TI is selected too short (TI_{-3}, TI_{-2} or TI_{-1}), the healthy myocardium presents a negative longitudinal magnetization value when the first α pulse is applied. Nevertheless, the measured SI corresponds to the magnetization magnitude, so in fact the healthy myocardium presents a higher signal intensity than the infarcted tissue. Thereby, as the TI becomes shorter, the signal of infarcted tissue will decrease until it reaches the null point. For an extremely short TI, the infarcted tissue appears null and the healthy myocardium enhanced (TI_{-3}). On the other side, an excessively long TI (TI_1, TI_2 or TI_3) can lead to a lack of contrast between tissues since the healthy myocardium signal

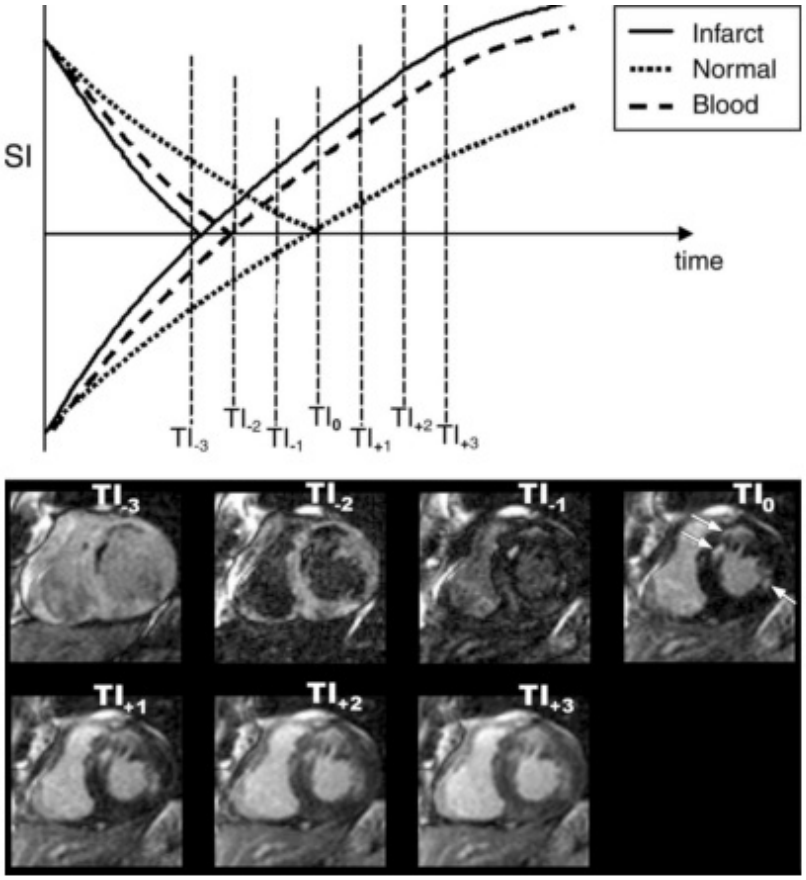

Figure 2.10: (Top) Signal intensity over time for three different tissue types: healthy myocardium, blood pool and infarcted tissue, considering multiple TI values. The signal magnitude directly depends on the TI chosen. (Down) DE-MR images correspondent to the different TI values [28].

is not null. Both tissues will present a positive SI and consequently less image contrast.

For the optimal TI (TI_0) the infarcted myocardium shows enhancement (image arrows) while the healthy myocardium presents a null signal [28].

However, even if all these limitations are compensated for, one major limitation remains. Since DE-MRI is cardiac triggered, irregular HR directly affects signal behaviour causing strong image artefacts.

In the theoretical situation where HR is completely steady, the interval between R-peaks is constant and so longitudinal magnetization has always the same time to recover. Therefore, the signal intensity (Ma) is the same for all cardiac cycles.

However if the R-R length varies, the amount of time for the longitudinal magnetiza-

tion to recover is different for each cycle (Fig. 2.11). If the R-peak occurs earlier than usual, the time available for Mz to recover is shorter than To. Therefore the Ma available at the next cycle will be higher. On the other hand, if the R-peak occurs later, Ma of the following cycle will have a lower intensity.

In summary, varying R-R lengths will lead to a variation of the acquired MR signal over several acquisition cycles.

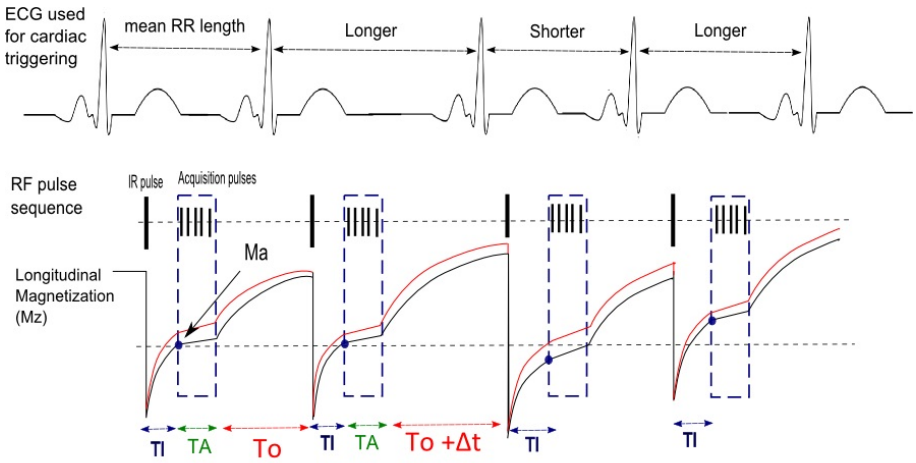

Figure 2.11: Schematic representation of Mz behaviour over time in a repeated IR acquisition considering two different tissue types: healthy myocardium (black solid line) and infarcted myocardium (red solid line). For a patient with irregular heart rate, the cardiac cycles present different lengths thereby influencing Mz behaviour.

Thereby when sampling K-space, different segments will be assigned with different signal intensities (Ma) depending on their correspondent acquisition window (Fig. 2.12).

As a result, sampling K-space with different signal intensities leads to strong artefacts when the final image is reconstructed.

To compensate for image artefacts due to HR irregularities is the main focus of this thesis.

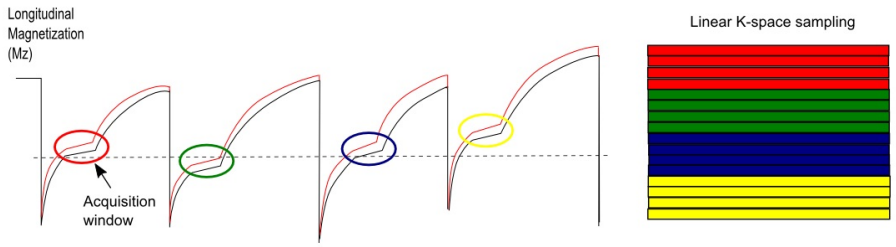

Figure 2.12: Schematic representation of Mz behaviour over time using a repeated IR acquisition with irregular heart rate. In each cardiac cycle an acquisition window (coloured circles) is considered where several data points are acquired. On the right side of the image a representation of K-space linear sampling is shown. Different segments of K-space are filled with data from their correspondent acquisition window. Different colouring of the segments/acquisition windows represents different signal intensities.

2.5.1 Minimization of image artefacts due to irregular HR

A wide range of correction methods has been presented through the literature with positive outcome in reducing image artefacts due to irregular HR and incorrect nulling of the myocardium.

A study by Krishnamurthy et al. reported positive results when applying a TI optimization method to reduce artefacts in arrhythmic patients [8]. The method consisted in dynamically adapting the TI for each acquisition cycle:

$$TI_{opt} = ln(2/(1 + exp(-RR/T1))) * T1 \tag{2.8}$$

Where R-R describes the length of the previous cardiac cycle and T1 the relaxation time of the tissue intended to be corrected. This formula was then used to accurately correct the myocardium signal. The study reported a decrease in artefacts intensity of 180 % with adaptive TI correction when compared without a correction method. Myocardium/blood CNR also showed an improvement of approximately 70% with TI correction.

Another recent study reported an alternative approach to dynamic TI optimization, where not only the TI is optimized for each cardiac cycle but also the inversion pulse angle (α_{IR}) is considered [7]. The degree of α_{IR} applied directly influences the amount of Ma available and thereby the final signal intensity acquired. Thereby, optimization of

not only the TI but also the α_{IR} can be useful to minimize signal irregularities.

TI optimization was be described by:

$$\Delta TI_{opt} = T1ln\left(\frac{e^{\frac{-T0}{T1}} - 2}{e^{\frac{-To-\Delta t}{T1}} - 2}\right) \tag{2.9}$$

Inversion pulse angles optimization was described by:

$$cos\Delta\alpha_{IR} = \frac{e^{\frac{-T0}{T1}} - 1}{e^{\frac{-T0-\Delta t}{T1}} - 1} \tag{2.10}$$

With this optimization method, the study reported a reduction in the myocardium signal deviation from the mean value of 15 % to $2,5\%$ [7, 9].

However, both of these TI optimization methods are T1 dependent according to Equations 2.8 and 2.9. Thereby, selection of the optimal TI that correctly nulls the healthy myocardium does not correspond to the optimal TI of the remaining tissues. Thus optimal correction of the healthy myocardium only reduces image artefacts arising from the healthy myocardium. Strong image artefacts may still arise due to signal variation of the non-corrected tissues.

Thereby, the proposed method in this thesis intends to compensate not only for a single tissue but multiple tissues simultaneously. By taking into account several tissues signals when optimizing the TI, artefacts arising from different tissue can be corrected and the overall artefacts level further reduced.

Chapter 3

IR DE-MRI simulation environment

3.1 Introduction and motivation

Due to DE-MRI wide range of medical applications and crucial role when assessing MI patients, demand on image quality and artefact compensation methods has increased.

Nevertheless, a major limitation remains when imaging irregular heart rate patients. If the heart rate is unsteady, signal intensity will be different for each acquisition cycle. In this case, different segments of K space are sampled with different signal intensities leading to strong artefacts when the final image is reconstructed (Section 2.5). The presence of such artefacts decreases image quality and misleads clinical diagnosis, thereby being of crucial importance to develop methods that aim to compensate for such artefacts.

Previous studies have presented compensation methods that dynamically adapt the TI in order to guarantee that the signal from healthy myocardium is always null. However, the choice of TI is T1 dependent and correcting for the healthy myocardium can still lead to artefacts arising from other tissues that were not corrected.

Therefore, this project intends to develop a novel artefacts reduction method that takes into account several tissue types. The main goal is to correct the TI for each cardiac cycle such that signal intensity remains as constant as possible. A multi-tissue approach is considered such that image artefacts arising from different tissue types can all be reduced simultaneously. In addition, the method also considers adapting two acquisition parameters (TI and α) to try to compensate for the maximum amount of artefacts possible.

For the purpose of this study, a simulation environment was built by the author, modelling 2D DE-MRI acquisition using a cardiac triggered IR sequence.

The following sections of the this chapter present the methodology and results obtained with the construction of such simulation environment.

3.2 Methodology

The built simulation environment comprehended several levels of organisation in different functions such as: *ECG triggering*, mathematical description of a repeated *IR sequence signal* (Section 3.2.1) and *2D image acquisition* (Section 3.2.2).

The first modular function, (*ECG triggering*), was responsible for generating a virtual ECG signal. Random time lengths between two consecutive R peaks were simulated with a standard deviation (10 to 50 %) around the mean heart rate [7]. Both the mean heart rate as well as the deviated distribution could be changed initially as input variables. Thus allowing to simulate multiple situations from a steady HR to a more irregular HR. This virtual ECG signal served as trigger to the following modular function (Section 3.2.1).

3.2.1 Mathematical description of a repeated IR signal

To allow for a quantitative prediction of the signal for different levels of HR irregularities, a second modular function (*IR sequence signal*) modelled the MR signal behaviour for an IR sequence (Section 2.4.3).

SI was determined taking into account the longitudinal magnetization at excitation prior to data acquisition (Ma) as well as sequential calculation of transversal magnetization (M_{xy}) and recovering longitudinal magnetization (M_z) over the acquisition window in consecutive cardiac cycles.

Longitudinal magnetization at excitation ($M_{z,n}$) of cycle (n) directly depends on the longitudinal magnetization available before the IR pulse at the end of the previous cycle (n-1) (M_{plus}) [7] :

$$M_{plus} = 1 + (M_{z,n-1} - 1)e^{\frac{-T_0-\Delta t}{T1}} \tag{3.1}$$

$$M_{z,n} = 1 + (M_{plus}cos(\alpha) - 1)e^{\frac{-TI}{T1}} \tag{3.2}$$

Where T_0 corresponds to the mean R-R interval length, α is the excitation flip angle and Δt describes the difference between the varying R-R length and the mean R-R length (T_0).

However during simulation implementation, the first cardiac cycle was set as an exception since there is no previous cycle to recover from. Thereby, longitudinal magnetization at acquisition ($M_{z,n}$) was set to [7]:

$$M_{z,n} = 1 + [(1 - e^{\frac{-To-\Delta t}{T1}})cos(180^{o})]e^{\frac{-TI}{T1}} \tag{3.3}$$

Nevertheless, equation 3.2 and equation 3.3 were only used to describe ($M_{z,n}$) for the first data point acquired in each acquisition window.

The following points were calculated considering how the longitudinal magnetization ($M_{z,n}$) recovers from the previous acquisition pulse (α) [35]:

$$M_{z,n} = M_{z,n-1}e^{\frac{-TR}{T1}}cos(\alpha) + M_{z0}(1 - e^{\frac{-TR}{T1}}) \tag{3.4}$$

Regardless of the data point, each longitudinal magnetization ($M_{z,n}$) is brought to the xy-plane and the transversal magnetization (M_{xy}) can then be calculated [35]:

$$M_{xy} = M_{z,n}e^{\frac{TE}{T2*}}sin(\alpha) \tag{3.5}$$

The number of repeated $M_{z,n}$ and M_{xy} calculations (data points acquired) per acquisition window was set by the variable N (Section 2.4).

Since acquisition lasts for a period of time (TA), it directly depends on the number of data points per window (N) and the time between consecutive excitations (TR):

$$TA = TR * N \tag{3.6}$$

Both the TR and N could be changed at the start of simulation as input variables.

3.2.2 Simulate 2D image acquisition

Signal behaviour at acquisition modelled earlier was then used to simulated 2D image acquisitions.

This third modular function (*2D image acquisition*) required as input the simulated ECG signal, the signal intensity previously calculated (Subsection 3.2.1), a numerical phantom and a K-space sampling trajectory.

A numerical phantom was implemented to mimic a short-axis view of the left ventricle representing three tissue types: fibrotic tissue, healthy myocardium and blood pool (Fig. 3.1).

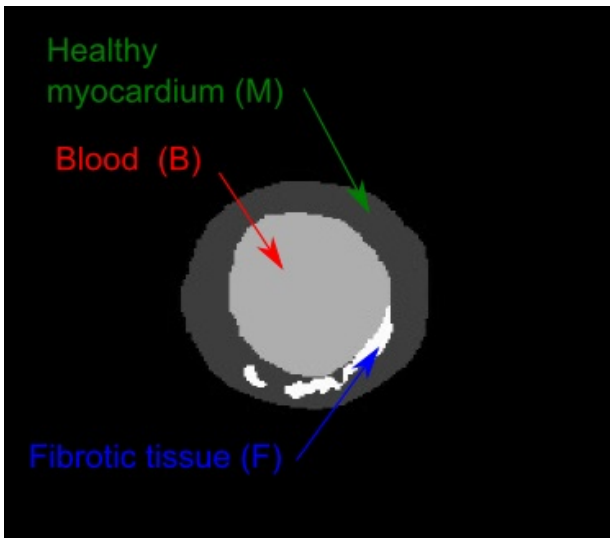

Figure 3.1: Numerical phantom used in the simulation environment representing a short-axis view of the left ventricle with three different tissue types: fibrotic tissue (F), blood pool (B) and healthy myocardium (M).

The phantom was manually outlined from a scan image and a mask set to define the outlines of each tissue. Each mask was assigned with intensity of 1 and the remaining background set to zero. However for representation purposes, in Fig. 3.1 the tissue masks were assigned different intensities.

Secondly, each tissue mask was assigned with the signal intensity calculated (Section 3.2.1) for the correspondent T1 value of that tissue. This was done for each data point individually, followed by the sum of the three tissue specific signal masks. To the final image thus obtained, a 2D fast Fourier transform (FFT) was applied resulting in the

Parameters	Value used
Mean heart rate	75 bpm
Matrix size	240 x 240 pixels
N factor	12 lines per window
Number of acquisition cycles	20
Fibrotic tissue (T1)	220 ms
Blood pool (T1)	310 ms
Healthy myocardium (T1)	550 ms
TE/TR	0/4.7 ms
Initial TI	270 ms
Initial excitation flip angle (α)	25 degrees
Start-up echoes	8
Upper boundary	[40,450]
Lower boundary	[0,150]

Table 3.1: Acquisition parameters used for simulations.

correspondent K-space matrix.

After this, the transformed K-space was modelled according to the chosen sampling trajectory, re-organizing data points by the order of acquisition set by the sampling trajectory. A simple linear cartesian trajectory was used in the simulation environment in similarity to the one used by the scanner. Finally, an inverse fast Fourier transform (IFFT) was applied to reconstruct the final image.

Parameter values used during simulation can be seen in Table 3.1. Upper and lower boundaries variables refer to a set of values defined during the TI optimization method; further description is available in Section 3.2.3. Since the T2* of the simulated tissues were unknown and for simplicity reasons, the TE was considered null. It was assumed that neglecting the T2 relaxation effect would not have a major effect on the final results, however it is a limitation of the simulation environment.

3.2.3 TI compensation method using a multi-tissue model

The method here suggested considers a multi-tissue approach of the dynamic TI optimization. The main purpose was to optimize TI such that signal intensity of several tissues remained as constant as possible.

This was achieved by minimizing the differences between the signal acquired with HR variation ($SI_{tissue,\%HRvariation}$) and the reference signal with no HR variation ($SI_{tissue,0\%HRvariation}$). This was accounted for using the Sum of Squared Error (SSE) for each tissue individually (SSE_{tissue}):

$$SSE_{tissue} = \Sigma(SI_{tissue,\%HRvariation} - SI_{tissue,0\%HRvariation})^2 \tag{3.7}$$

Since a multi tissue approach was considered, the sum of squares total error (SSE_{total}) was calculated taking into account the (SSE_{tissue}) not only for the healthy myocardium but for multiple tissues.

All three tissue types could have been taken into account, nevertheless from signal behaviour results further discussed in Section 3.3.1, only the blood pool and healthy myocardium were considered for the correction:

$$SSE_{total} = W * SSE_{myocardium} + (1 - W) * SSE_{blood} \tag{3.8}$$

Where W (weighting factor) allows to correct more strongly for artefacts arising from the healthy myocardium ($W > 0.5$) or from the blood pool ($W < 0.5$).

Thereby the main idea was to determine the optimal acquisition parameters (TI_{opt} and α) that correspond to the minimization of the (SSE_{total}) which minimises irregularities in Ma.

A MATLAB integrated script called *fminsearchbnd* was used to calculate the optimized parameters. *fminsearchbnd* allows to search for the local minimum (X) around an initial value (X0) of an input function (fun) with a set of upper and lower boundaries (LB,UB):

$$[X] = fminsearchbnd(fun, X0, LB, UB); \tag{3.9}$$

In this study, this function was used for searching the value of TI (TI_{opt}) that corresponds to the minimum of the function (SSE_{total}):

$$[TI_{opt}, \alpha] = fminsearchbnd(SSE_{total}, parameters_{initial}, LB, UB) \tag{3.10}$$

Where the array $parameters_{initial}$ defined the initial parameters values around which the function searches for a solution and $[LB, UB]$ was the set of boundaries for the parameters search. Specific values used for these variables are shown in Table 3.1.

In addition to only optimizing the TI, another scenario was also tested where both acquisition parameters (TI and α) were optimized. Thus intending to study the effect of optimizing the flip angles as a way to further improve image quality. In the Table 3.1, UB and LB refer to the values used when optimizing both the TI and the excitation flip angle (α) simultaneously, where [0,40] boundaries refer to α and [150, 450] to TI. In the case where the optimization of the TI was considered, UB and LB only included the values [150] and [450].

3.2.4 Evaluation of signal deviation and image artefacts

The effect of irregular heart rate in signal behaviour was quantified by calculation of the signal standard deviation. The standard deviation allowed to quantify how much the signal deviates (σ) from the mean (μ) signal [36]:

$$\sigma = \sqrt{\frac{1}{N}\sum_{i=1}^{N}(x_i - \mu)^2} \tag{3.11}$$

To obtain signal deviation percentage wise, σ was divided by μ and multiplied by 100.

Secondly, a method was devised to quantify image artefacts intensity (Fig. 3.2). A reference image (simulated with steady HR) was subtracted to each simulated image with HR variation. Thus obtaining an image that solely holds the artefacts intensity (Fig.3.2 (c)). The overall artefacts intensity was quantified by calculating the mean value of this final image.

This quantification method of artefacts level was used to compare the our TI optimization method with non-corrected images.

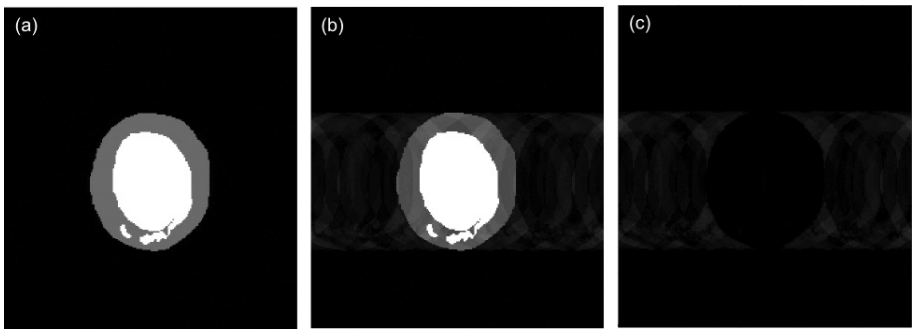

Figure 3.2: (a) Simulated 2D image of the left ventricle considering a steady heart rate. (b) Image simulated for 30% HR variation. Gray scale was adapted to visually enhance image artefacts. (c) Image solely holding the artefacts intensity obtained subtracting image (a) from image (b).

3.3 Results and discussion

3.3.1 Influence of irregular HR on signal behaviour and image quality

Simulation of a repeated IR signal acquisition according with the experimental methodology described in section 3.2.1 was successfully accomplished. Signal intensity curves were simulated with steady heart rate (reference signal) and with heart rate variation.

Reference signal along each acquisition window acquired with no heart rate variation can be seen in Fig. 3.3 (a,b,c). As expected for a regular HR, all signal curves within each tissue type showed the same intensity (signal curves overlap) meaning Ma remained constant for all cycles.

For 30 % heart rate variation and no method of correction, signal curves showed different intensities and no longer overlap (Fig. 3.3 (d,e,f)). This means that Ma was irregular and the acquired signal presents different intensities.

In order to quantify the effect of irregular HR in signal behaviour, signal variation was measured (Section 3.2.4) for all three tissue types considering different HR variation values (Fig. 3.4).

Results shown that both HR variation and signal variation present a direct relation, where a higher HR variation leads to a higher signal deviation, specially for the myocardium (ex: 50 % HR relates to almost 90% signal deviation).

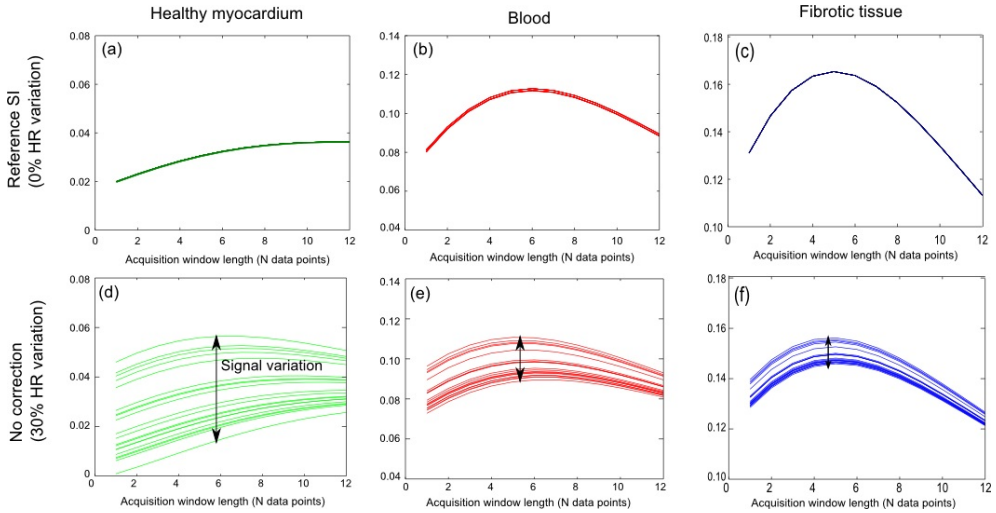

Figure 3.3: Signal intensity (Y axis) along each acquisition window (X axis - 12 data points per window) obtained through numerical simulation for three different tissue types: healthy myocardium (green), blood pool (red) and fibrotic tissue (blue). (a,b,c) Reference signal acquired with no heart rate (0 %) variation. (d,e,f) Signal acquired with heart variability (30 %) and no method of correction applied. Signal variation is present when HR is unsteady.

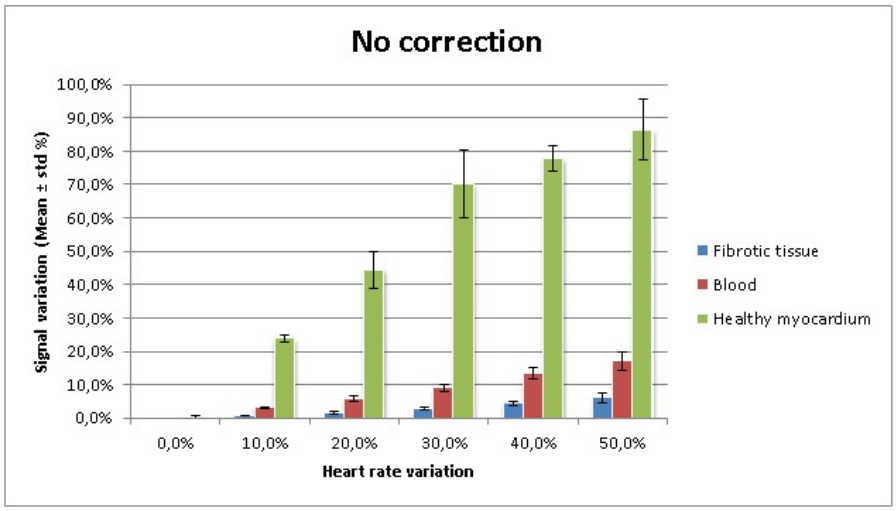

Figure 3.4: Measurements of signal variation (Y-axis) from simulated data as a function of heart rate variation (X-axis) for the three tissue types.

In addition, it was also concluded that HR variations seem to lead to a much stronger signal variation for the blood and the myocardium rather than the fibrotic tissue. Therefore, when implementing the multi-tissue TI optimization method (Equation 3.8), only the blood and healthy myocardium signals were taken into consideration. Further results

referring to the implementation of the TI correction method are presented in the following Section 3.3.2.

Secondly, 2D DE-MRI images were simulated (Section 3.2.2) using a numerical phantom and previously generated signal intensity curves.

2D simulated images representing short-axis view of the left ventricle can be seen in Fig. 3.5. A reference image was simulated with 0 % heart rate variation where no artefacts are visible (Fig. 3.5 (a)). The fibrotic tissue appears hyperenhanced compared to the healthy myocardium (close to null) and the blood pool presents intermediate signal intensity, as expected with delayed enhancement theoretical background. In addition, analysis of Fig. 3.5 (a) confirms that a constant signal variation leads to an artefact-free image since K-space was filled with a constant Ma.

On the contrary, for 30 % heart rate variation, artefacts were visible along the phase encoding direction (Fig. 3.5 (b)). Therefore, irregular signal behaviour (Fig. 3.3 (d,e,f)) can be directly related with the presence of artefacts in the final image. The artefacts, visually enhanced with a different gray scale, can be seen in Fig. 3.5 (c).

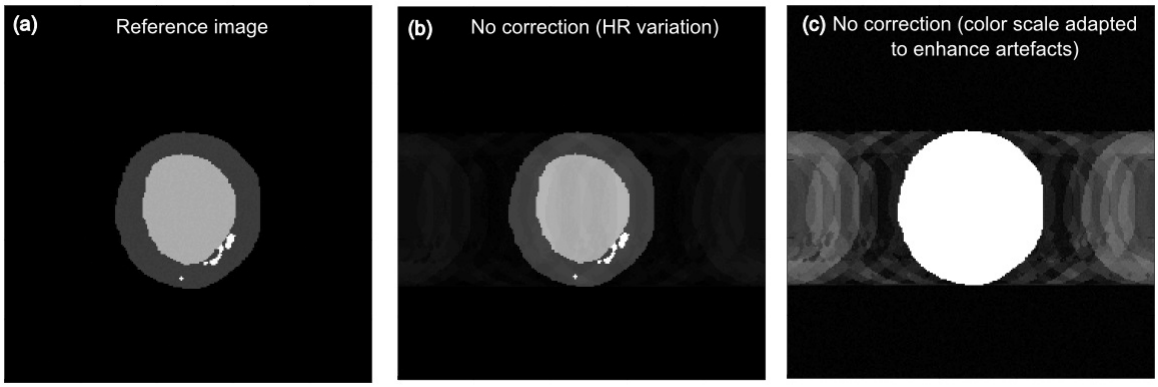

Figure 3.5: 2D images obtained through numerical simulation representing short-axis slice of the left ventricle. (a) Reference image obtained with steady heart rate (0 % variation). The infarcted myocardium showed enhancement compared to an almost nulled healthy myocardium signal. (b) Image acquired with 30 % heart rate variation and no method of correction. Ghosting artefacts are visible along the phase encoding direction of the image. (c) Image acquired with 30 % heart rate variation and no method of correction. Gray scale was adapted to visualize image artefacts.

3.3.2 Image artefacts reduction: dynamic TI optimization

The present subsection refers to the results obtained using the TI optimization method previously described in Section 3.2.3. Two approaches were simulated, optimizing the TI with a multi-tissue approach and for a single tissue, for comparison purposes to our method.

Signal intensity curves were successfully simulated for 30% HR variations with TI correction method.

Fig. 3.6 shows SI curves behaviour after TI optimization was used.

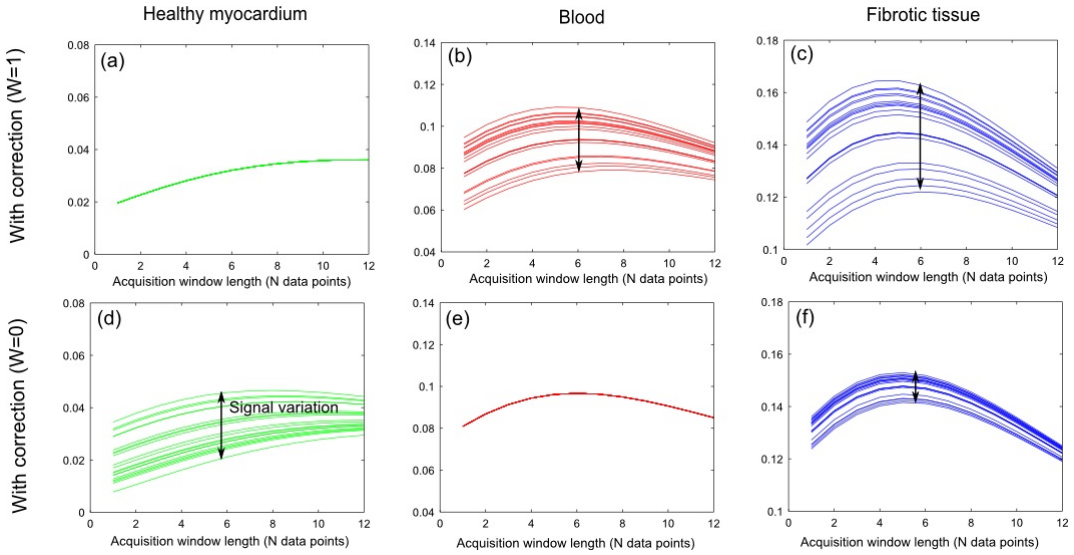

Figure 3.6: SI curves obtained through numerical simulations for three different tissue types: healthy myocardium (green), blood pool (red) and fibrotic tissue (blue) with 30% HR variation. (a,b,c) TI optimization applied according to Equation 3.8 with W=1 (correcting for myocardium). (d,e,f) TI optimization applied according to Equation 3.8 with W=0 (correcting for blood).

However, these two first cases refer to using only one tissue signal in the correction method. According to Equation 3.8, if W=1, only the healthy myocardium signal is corrected. Fig. 3.6 (a,b,c) shows that myocardium SI curves overlap since TI optimization made Ma constant over all cycles. Nevertheless, since only the myocardium signal was taken into account for the correction, both the blood and fibrotic tissue still showed signal variation.

On the other hand if W=0, only the blood signal was corrected. Fig. 3.6 (d,e,f)) shows

HR variation (%)	Fibrotic tissue	Blood	Myocardium
10	0,93 ± 0,14	0,0 ± 0,0	13,10 ± 1,37
20	2,02 ± 0,17	0,0 ± 0,0	23,63 ± 0,72
30	3,07 ± 0,15	0,0 ± 0,0	43,87 ± 2,78
40	2,45 ± 0,42	0,0 ± 0,0	40,85 ± 3,42
50	5,59 ± 0,56	0,0 ± 0,0	67,19 ± 6,38

Table 3.2: Signal variation measurements for different HR variation values considering the three tissue types: fibrotic tissue, blood and healthy myocardium. TI optimization method for W=0 was considered.

HR variation (%)	Fibrotic tissue	Blood	Myocardium
10	3,22 ± 0,24	3,78 ± 0,24	0,0 ± 0,0
20	7,17 ± 0,38	8,53 ± 0,32	0,0 ± 0,0
30	11,22 ± 1,91	13,20 ± 1,96	0,0 ± 0,0
40	17,28 ± 1,70	19,21 ± 1,99	0,0 ± 0,0
50	26,69 ± 2,29	29,47 ± 3,76	0,0 ± 0,0

Table 3.3: Signal variation measurements for different HR variation values considering the three tissue types: fibrotic tissue, blood and healthy myocardium. TI optimization method for W=1 was considered.

the opposite situation where the blood SI curves overlap since Ma was made regular. Both the healthy myocardium and fibrotic tissue SI curves still show signal variation.

Further signal variation measurements were performed for different HR variation values when applying W=0 and W=1 corrections. If W=0 (Table 3.2), blood signal shows 0% variation while other tissues show high level of variation (myocardium shows around 70% for 50% HR variation). If W=1 (Table 3.3), the myocardium signal shows steady signal measurements while both fibrotic tissue and blood show variation (blood presents 30 % for 50 % HR variation). The present measurements seem to indicate that correcting solely for one tissue type led to the presence of strong signal variation from the remaining non-corrected tissues. In addition, correcting only for the healthy myocardium led to a higher signal deviation of the fibrotic tissue even comparing with no correction method.

Thereby, our multi-tissue TI optimization approach intends to look for a W factor (0<W<1) that finds the best balancing correction between blood and myocardium signals, relating to the maximum artefacts reduction possible.

In order to determine the best W factor, artefacts intensity level was measured for different W values. Firstly, the artefacts intensity level measured for different W values from the signal contribution of each tissue individually can be seen in (Fig. 3.7 (a)). Similarly to signal behaviour results, if W=0, artefacts mainly arise from the healthy myocardium since the blood signal is corrected. And if W=1, the artefacts mainly arise due to the blood pool and a smaller portion due to the fibrotic tissue. Since at W=0 and W=1 the signals of blood and myocardium respectively were corrected, it should be expected that for both W values, the artefacts level should be zero for the respective tissues. However, a random level of noise was added to the simulated images and therefore the slight detection of artefacts (intensity = 0.2) is due to the noise and not artefacts specifically arising from the tissues since we measured the mean of the image background.

Secondly, evaluation of the artefacts intensity level measured when summing all tissues together can be seen in Fig. 3.7 (b). A high level of artefacts was observed at W=0 and W=1 since correcting for only one of the tissues created artefacts arising from the remaining tissues. The best W factor, correspondent to the minimum amount of artefacts, was estimated as W=0.4.

Now considering W=0.4 as the best weighting factor, two methods of compensation were analysed comparing the optimization of only the TI parameter or optimization of both the TI and α.

One important aspect to keep in mind is that for the optimization of the excitation flip angles (α), a ramp-up approach with start-up echoes was considered. This means that only the last flip angle applied is optimized with our method. The remaining flip angles along within the same acquisition window are then scaled towards the last pulse (which was optimized). Thus 8 start-up pulses are calculated (beginning with 0^o) plus 12 (N factor) more that correspond to the number of segments acquired per acquisition. This type of implementation is more realistic and similar to what the scanner performs.

Measurements of signal variation for different HR variation values using both methods of compensation can be seen in Fig. 3.8. It was concluded that for lower values of HR

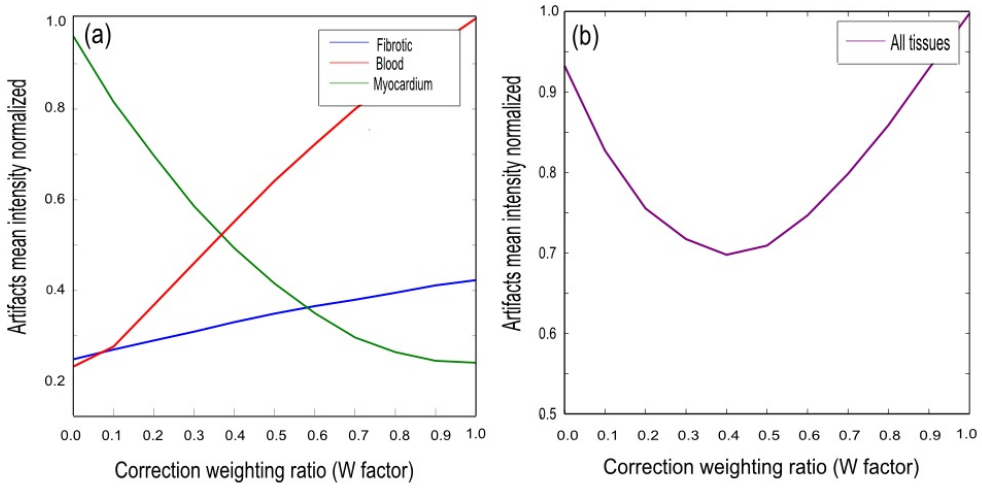

Figure 3.7: Artefacts mean intensity level (Y-axis) measured for different W factors (X-axis) considering 30% heart rate variation. (a) Measured for the three tissues individually. (b) Measured for the sum of all tissues.

variation, correction with only the TI or with both parameters showed similar signal variation for all three tissue types. On the other hand, for higher irregularities of the HR ($> 40\%$), correction with both parameters showed to further reduce signal variation. This was specially verified for the healthy myocardium where for 50 % HR variation, only TI optimization resulted in 35% signal deviation while optimization with both parameters reduced signal deviation to less than 25%. This can be explained by the fact that for a higher HR variation, the non-corrected signal presents more variation since both factors are correlated. Therefore the effect of adding the α parameter is more visible and further improves signal correction.

Thus further results were simulated/acquired considering optimizing both acquisition parameters to further reduce signal variation and image artefacts.

After determining the W=0.4 as the best weighting factor, a comparison can be made with the non-corrected SI curves (Fig. 3.9). SI irregularities of the blood and myocardium were compensated for successfully. Both signal curves (Fig. 3.9 (d,e)) showed less variation in intensity comparing with the non-corrected curves (Fig. 3.9 (a,b)). Fig. 3.9 (c,f) shows that signal variation for fibrotic tissue at W = 0.4 is slightly larger than with no correction method. This increase is outweighed by the improvement in reducing artefacts caused by the myocardium and blood.

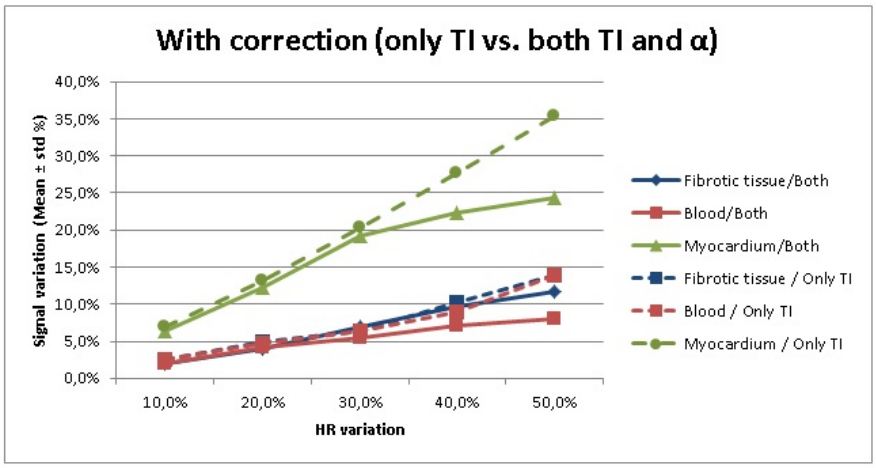

Figure 3.8: Signal variation (Y-axis) measured for different HR variation (X-axis) values for the three tissue types: healthy myocardium (green), blood pool (red) and fibrotic tissue (blue). Two correction methods were under consideration: optimizing only the TI (dashed lines) or optimizing both acquisition parameters (solid lines).

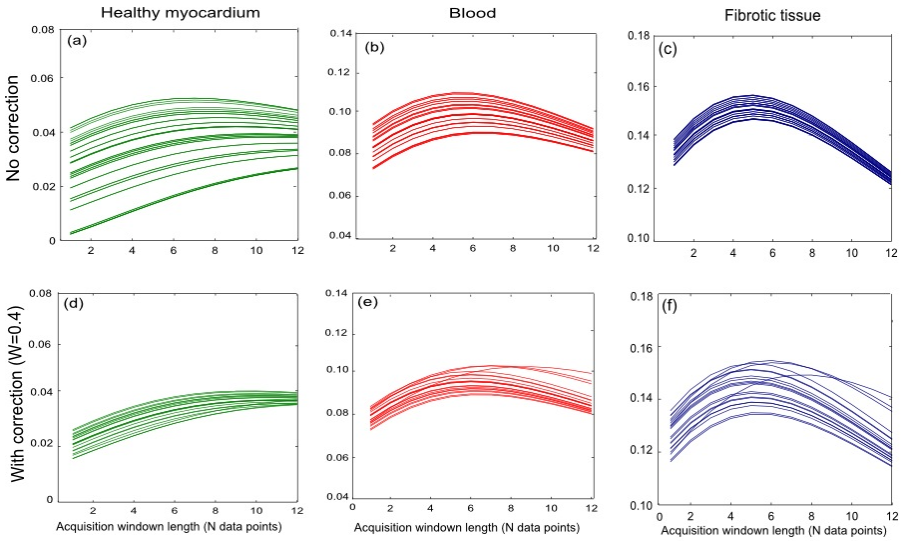

Figure 3.9: SI curves obtained through numerical simulations for three different tissue types: healthy myocardium (green), blood pool (red) and fibrotic tissue (blue). (a,b,c) Signal along each acquisition window acquired with heart variability (30 %) and no method of correction applied. (d,e,f) Signal along each acquisition window acquired with heart variability (30 %). TI and α optimization was applied with W=0.4.

Signal variation measurements (Fig. 3.10) lead to similar conclusions . A multi-tissue approach proved to greatly reduce signal variation for both the blood and myocardium

in comparison with absence of a correction method (Fig. 3.4) . For example, for 50% HR variation, the myocardium signal showed a reduction from 90% to approximately 25% while blood showed a reduction from 20% to less than 10%.

It was also verified that for the same HR variation, the fibrotic tissue signal showed a slight increase from 5% to a little over 10% when applying the TI correction method. This was expected since the fibrotic tissue signal was left uncorrected and thereby susceptible to the HR irregularities, however the increase in signal variation is minimal.

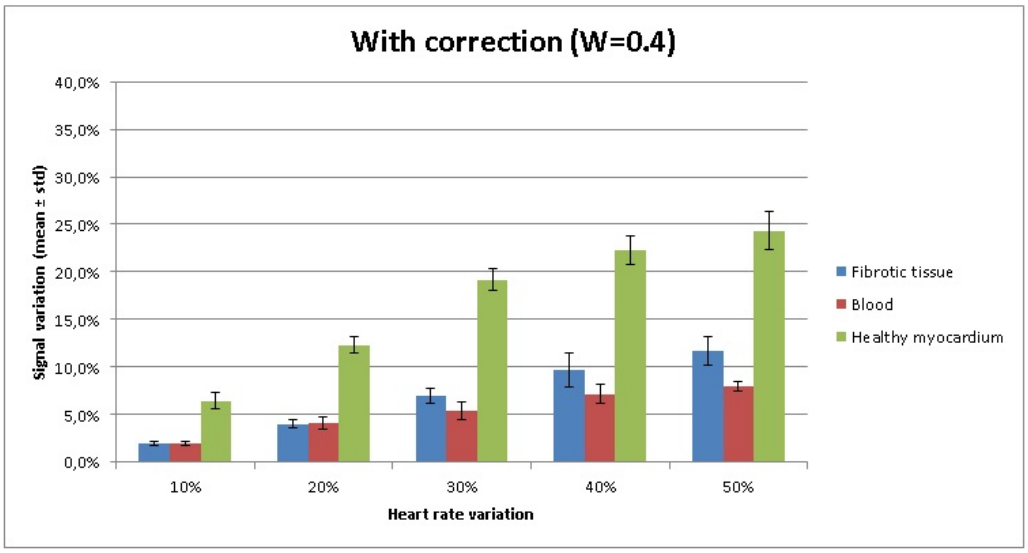

Figure 3.10: Signal deviation measurements (Y-axis) for simulated data over different HR variation values (X-axis). Measurements were made for all three tissue types.

Lastly, a reduction in signal variation with the TI optimization method resulted in final simulated images with less visible artefacts.

2D simulated images with different W values can be seen in Fig. 3.11. Image corresponding to the best W factor (Fig. 3.11 (c)) seems to present less artefacts than the other two.

Measurements of image artefacts level for different W values according to methodology described in Section 3.2.4 were performed and previously shown in Fig. 3.7 (b). Measurements of the simulated images showed that our multi-tissue approach (W=0.4) image (Fig. 3.11 (c)) presented 70% less artefacts than a non-corrected image at 30% HR variation. Corresponding to 20% less than W=0 (Fig. 3.11 (a)) and 30% less than W=1 (Fig. 3.11 (b)).

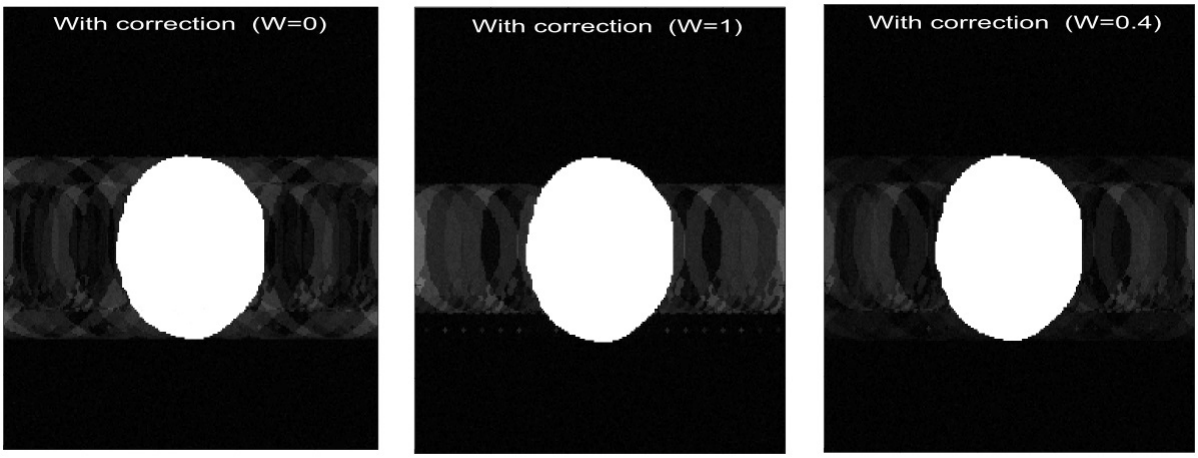

Figure 3.11: 2D images obtained through numerical simulation representing short-axis slice of the left ventricle. All images were obtained with 30 % heart rate variation and gray scaling was adapted to visually enhance artefacts. Correction method was applied with different W values: W=0 (a) , W=1 (b) and W=0.4 (c).

In conclusion, the idea to keep in mind is that a multi-tissue tissue approach showed not only to greatly reduced signal variation and image artefacts but to possible overcome a single tissue approach. However, studies with phantom experiments (Chapter 4) were necessary in order to validate conclusions drawn from simulated data.

Chapter 4

Phantom experiments

4.1 Introduction and motivation

The simulation experiments discussed in the previous chapter were evaluated on a clinical 3T MR scanner (Philips Healthcare, Best, The Netherlands) using gel tube phantoms.

4.2 Methodology

The multi-tissue correction approach was implemented on a clinical 3T MR scanner. Scan experiments were performed using three gel phantom tubes representing the fibrotic tissue, blood pool and healthy myocardium. Corresponding T1 values and other parameters used for the phantom experiments are shown in Table 4.1.

The same virtual ECG signals used in the simulation were considered as triggering and manually inserted into the scanner console when acquiring phantom data. The optimized parameters for the multi-tissue approach were pre-calculated to ensure similar conditions as the ones used in the simulations.

1D scan projections (Fig. 4.1) obtained at the scanner were used to calculate signal intensity curves over each acquisition window.

The scan projections have a width correspondent to the width of each gel tube and height correspondent to the total number of data segments necessary to sample one K-space matrix. Each line is a projection of the signal intensity acquired for a single data point onto the x-axis. The scanner organizes the data so that all first points acquired for

Parameters	Value used
Mean heart rate	75 bpm
Matrix size	240 x 240 x 8
N factor	12 lines per window
Number of acquisition cycles	20
TE/TR	2.26/4.7 ms
Fibrotic tissue (T1)	220 ms
Blood pool (T1)	450 ms
Healthy myocardium (T1)	650 ms
TI	270 ms
Initial excitation flip angle (α)	25 degrees
Start-up echoes	8

Table 4.1: Acquisition parameters used for phantom experiments acquisition.

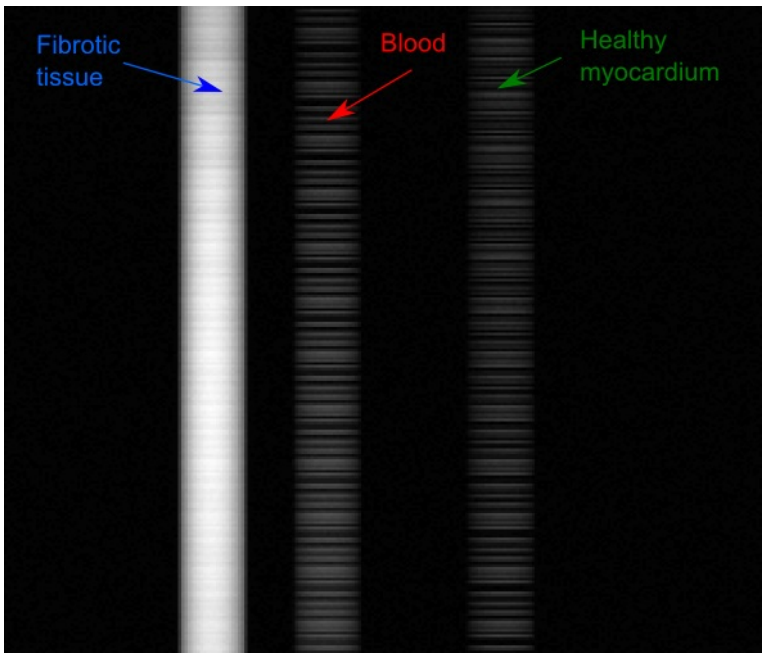

Figure 4.1: Example of a 1D scan projection image acquired with 30% HR variation using three gel phantoms representing the fibrotic tissue (left), the blood pool (middle) and myocardium (right).

all acquisition cycles are together (bottom rows) followed by all the second data points acquired for all cycles and so on. Thereby the last set of lines (top rows) will then represent the last data points for each acquisition cycles.

Measurements of each line in this 1D scan image allowed to obtain signal intensity curves for each acquisition window similar to the ones obtained with the numerical simulation.

In addition, 2D images were also acquired with and without using the multi-tissue correction approach for different W factors.

4.3 Results and discussion

4.3.1 Comparison to simulated signal behaviour

Firstly, in order to validate the simulation environment previously built, signal intensity along each acquisition window for a steady HR was obtained through simulation environment and phantom experiments for different (α) values. For this situation, a different N factor was considered (23 data points per window), however these measurements served only to support simulation validity and not to be included in any main results. For all further results, a N factor of 12 data points was used.

Fig. 4.2 shows similar curve behaviour between the simulated and acquired data for all flip angle values. Thus validating the built simulation environment and proving to be a real model of how the signal behaves in a real acquisition. As consequence, further conclusions retained from the simulation data were considered to be reliable.

For the first set of experimental results, images of gel phantom tubes acquired with 1D scan mode can be seen in Fig. 4.3. For a steady HR, signal intensity is stable over all acquisition windows thereby all data points within the same order position (all first points, all seconds...etc.) present the same intensity. On 1D scan images this reflects as a smooth transition of gray scale along the 1D scan length (Fig. 4.3 (a)). On the other hand, with 30% HR variation, the signal is irregular and thereby data points within the same order present different intensities presenting a striped pattern in a 1D scan image (Fig. 4.3 (b)).

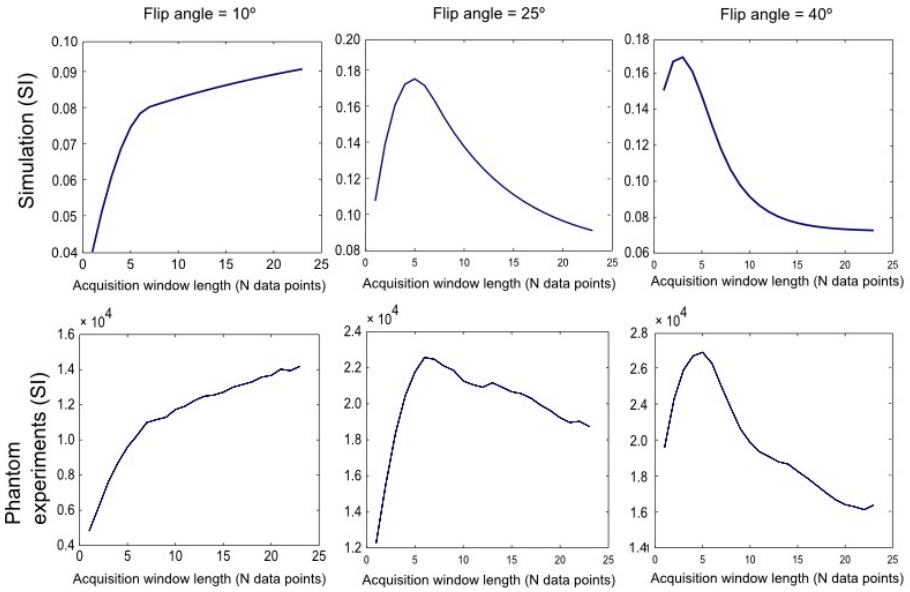

Figure 4.2: Signal intensity curves for the fibrotic tissue considering a steady HR obtained through the simulation environment (top row) and with phantom experiments (bottom row).

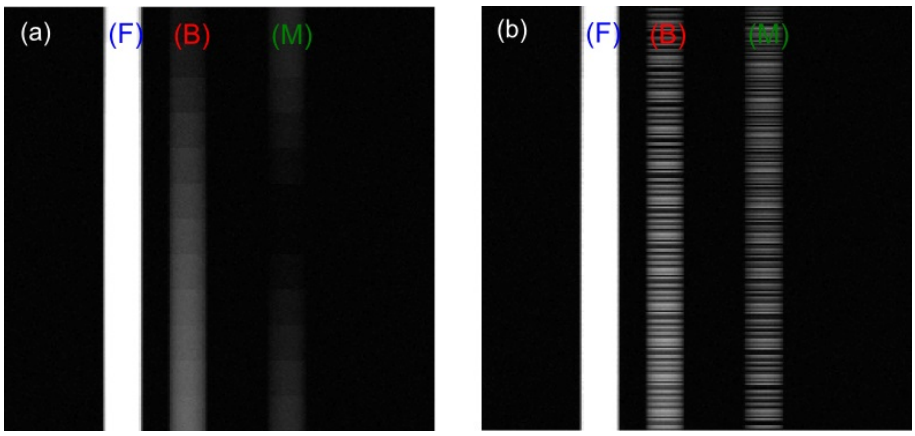

Figure 4.3: Image of 1D scan projections of three gel phantoms representing fibrotic tissue (left), blood pool (middle) and healthy myocardium (right). (a) No heart rate variation (b) 30 % HR variation.

Secondly, signal intensity curves similar to the simulated ones, were obtained by measurements of the 1D scan images. Acquired SI curves showed overlapping signal curves for a steady HR situation (Fig.4.4 (a,b,c)) and signal variation at 30% HR variation (Fig. 4.4 (d,e,f)). Again, a stronger variation in signal intensity was found for blood pool and myocardium rather than for the fibrotic tissue.

In order to quantify the effect of HR variation in the acquired signal behaviour, mea-

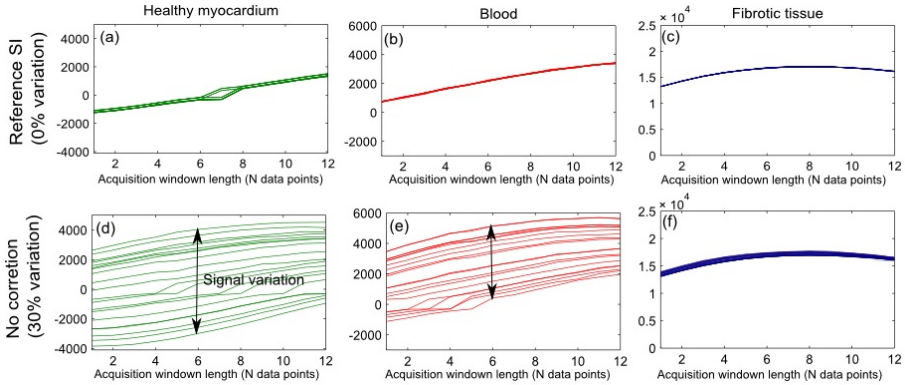

Figure 4.4: Signal measurements from 1D scan projections for three tissue types: healthy myocardium (green), blood pool (red) and fibrotic tissue (blue). (a,b,c) Reference signal along each acquisition window acquired with no heart rate (0%) variation (d,e,f) Signal along each acquisition window acquired with heart variability (30 %) and no method of correction applied.

surements of signal variation were performed as a function of different HR variation values (Fig. 4.5). While for a steady HR, the signal showed negligible variation, a considerable signal variation was visible specially for the blood pool and healthy myocardium for higher values of HR variation. A slight difference was visible comparing to the same results obtained for the simulated data (Fig. 3.4). It appears that the blood pool showed a much higher signal variation in the phantoms experiments than in the simulation. This effect is most probably due to deviation between the T1 value used at the simulation and the T1 from the gel tube used for the experiments. However, a similar behaviour between the two data types is still visible since the presence of HR variation directly relates to a higher signal variation and the fibrotic tissue showed negligible variation compared with the remaining tissues.

Thereby confirming the previously described conclusions, phantom experiments data seem to confirme that HR variations lead to higher SI irregularities for healthy myocardium and blood than for fibrotic tissue. Thus, implementation of the correction method (Section 3.2.3) only took into account the signal from myocardium and blood.

In addition, the 2D images acquired with phantom experiments can be seen in Fig. 4.6.

The reference image shows three phantoms with T1 values similar to the ones used on the simulated results (Fig. 4.6 (a)). Moreover as expected, the fibrotic tissue showed

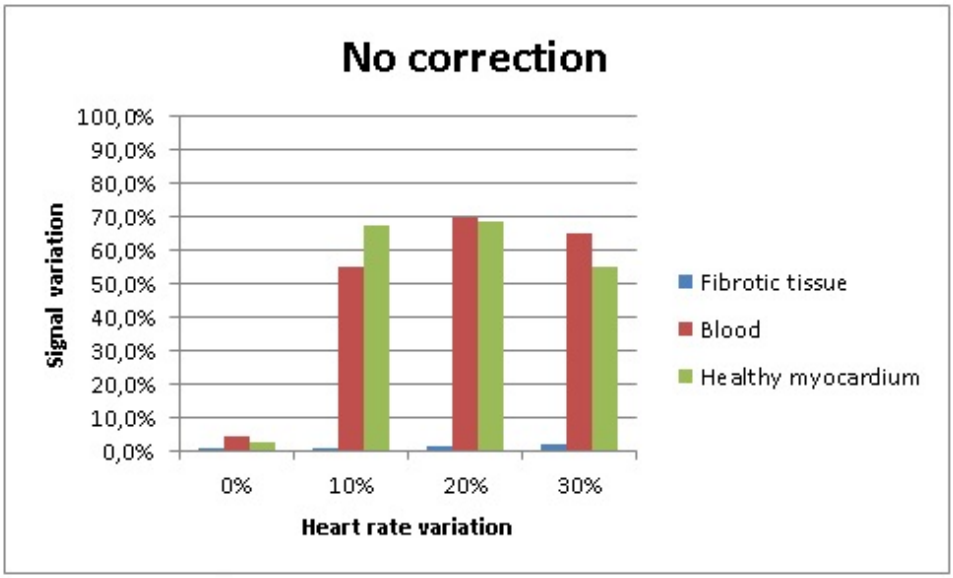

Figure 4.5: Measurements of signal variation (Y-axis) from phantoms experiments as a function of hear rate variation (X-axis) without correction for the three tissue types.

hyperenhancement while the healthy myocardium showed a nulled signal. In addition, an enhancement of the edges was visible for the myocardium phantom image. This can be explained by the transient TI effect. The selected TI is set to null the myocardium at the beginning of the data acquisition. Nevertheless, data was acquired for 12*TR (56.4 ms) and during data acquisition the magnetization of the myocardium recovers further leading to a signal from the myocardium greater than 0. At the end of the acquisition window, the higher k-space frequencies are sampled with a non-null signal intensity, which represent the fine details and edges of an image.

For 30 % HR variation and no correction applied, the scanner image shows a high level of artefacts mainly arising from blood pool and myocardium (Fig. 4.6 (b)). Again, a direct relation can be set between irregularities in myocardium and blood signals (Fig. 4.4 (d,e)) and image artefacts arising from the same tissue types (Fig. 4.6 (b)).

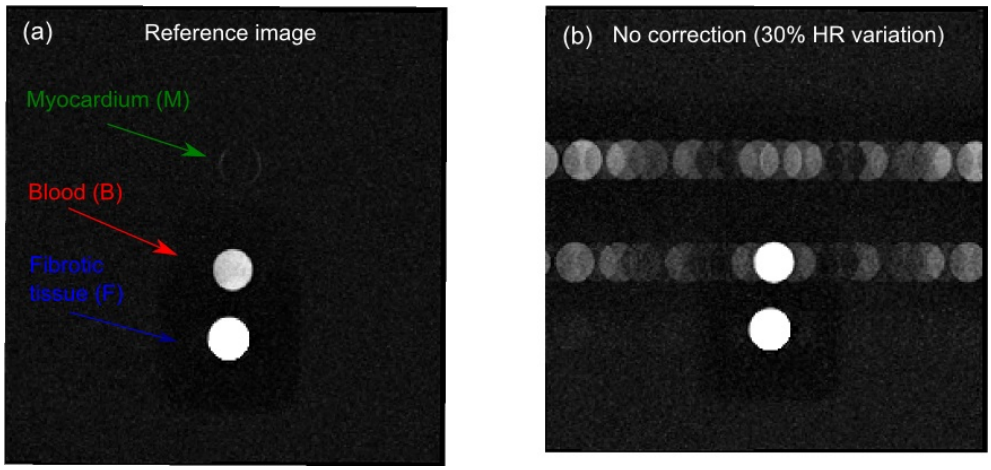

Figure 4.6: 2D images acquired at 3T using experimental tube phantoms. (a) Reference image obtained with steady heart rate (0 % variation). Each circle represents one tissue type according to their T1 values: fibrotic tissue (bottom), blood pool (middle) and healthy myocardium (top). (b) Image acquired with 30 % heart rate variation and no method of correction. Strong artefacts are visible arising from the blood pool and healthy myocardium.

4.3.2 Image artefacts correction : dynamic TI optimization

Implementation of the TI optimization method with similar parameters was successful in a 3T clinical scanner.

Experimental SI curves obtained with TI correction for W=0 and W=1 can be seen in Fig.4.7. Improvements in signal variation can be seen for blood signal curve at W=0 (Fig. 4.7 (b)) and equally for the myocardium signal curve at W=1 (Fig. 4.7 (d)). Nevertheless, complete correction of signal variation was not possible similar to what was observed in the simulated results (Fig. 3.6). The T1 times of the gel phantoms were previously determined using a Look Locker sequence [31]. Nevertheless, the incomplete correction of the signal from the myocardium suggests that the T1 time of myocardium was not determined correctly and thus the wrong T1 time value was used in the correction formula.

Artefacts measurements for each tissue individually (Fig.4.8 (a)) showed similar conclusions to the simulated data. If W=0, artefacts arise mainly from healthy myocardium while if W=1, artefacts arise from the blood signal. In addition similarly to simulation data, for W=0 and W=1, the level of artefacts for the blood and the myocardium respec-

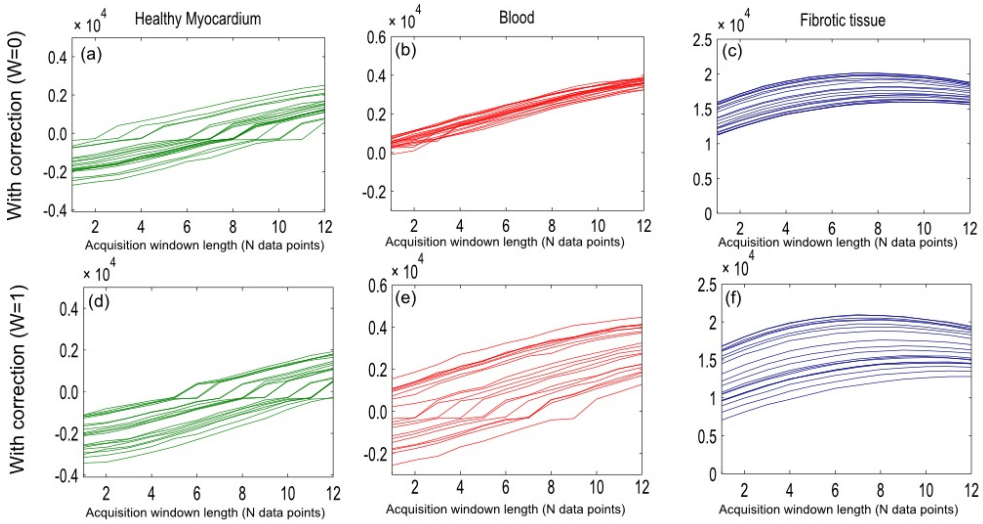

Figure 4.7: SI curves obtained through phantom experiments for three different tissue types: healthy myocardium (green), blood pool (red) and fibrotic tissue (blue) with 30% HR variation. (a,b,c) TI optimization applied according to Equation 3.8 with W=0 (correcting for blood). (d,e,f) TI optimization applied according to Equation 3.8 with W=1 (correcting for myocardium).

tively, is never zero due to the presence of random noise in the acquired images. Artefact level for different W values considering the sum of all tissues confirmed the best weighting factor to be 0.4 (Fig. 4.8 (b)). The scan results seem to suggest that the multi-tissue approach (W=0.4) reduces the overall artefacts amount by more than 20-40 % compared to a single-tissue correction approach.

Thereby, assuming W=0.4 as the best W factor, reflected in less deviated signal intensity curves (Fig. 4.9). Both healthy myocardium and blood signal curves with TI correction (W=0.4) present less variation than with no correction.

Then, measurements of signal variation for different HR variation values considering a TI correction of W=0.4 and with both acquisition parameters (TI and α) were performed for the scan experiments (Fig. 4.10). The multi-tissue approach revealed to greatly reduce signal variation when comparing to the non-corrected situation (Fig. 4.5). For example, for 30% HR, the blood presented a reduction from 70% to less than 40%. While for the same situation, the healthy myocardium showed a reduction of signal variation from 55% to less than 30%. The same phenomenon of increase in signal variation of the fibrotic tissue was visible when correcting for W=0.4 since it it's signal was left uncorrected.

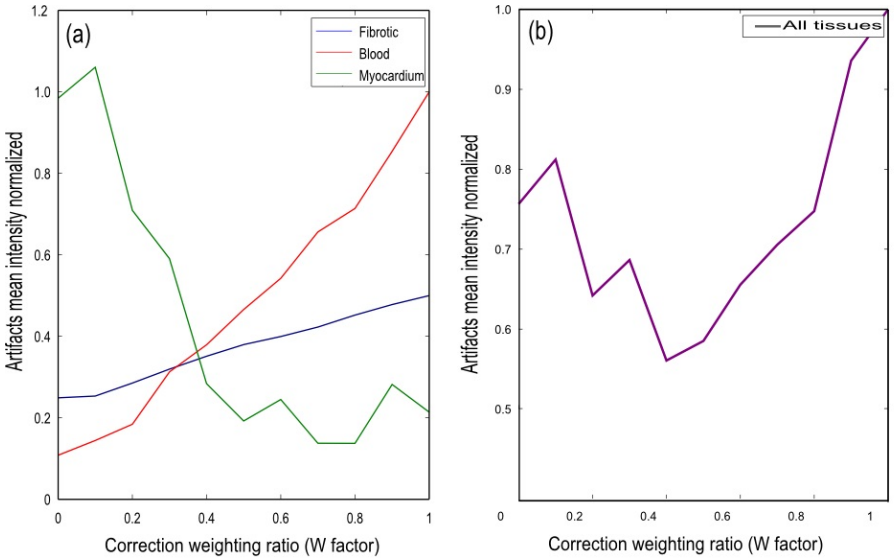

Figure 4.8: Artefacts intensity measured for different weighting values (W) for each tissue individually (a) and summing all tissues (b).

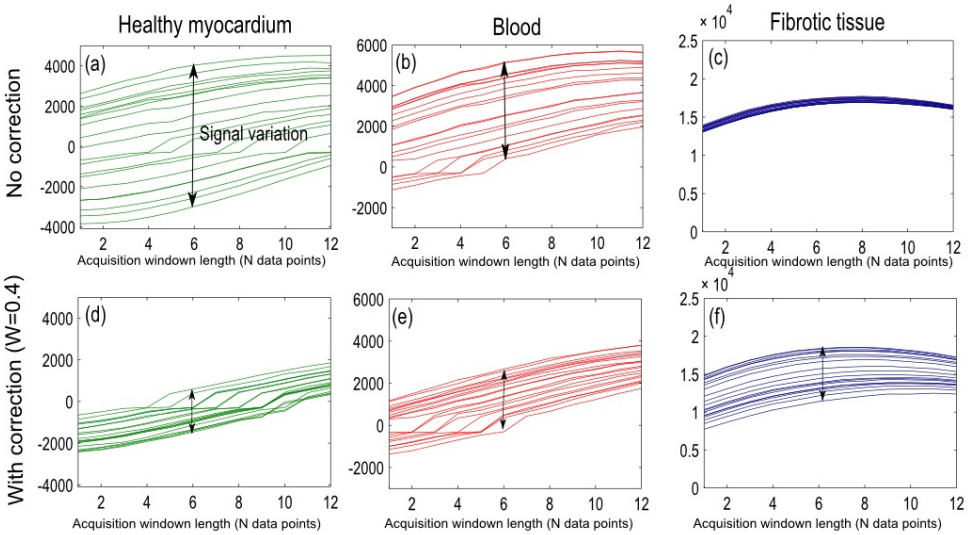

Figure 4.9: Signal intensity for data acquisition through 1D scan projections from gel phantoms representing the three different tissue types: healthy myocardium (green), blood pool (red) and fibrotic tissue (blue). (a,b,c) Signal along each acquisition window acquired with heart variability (30 %) and no method of correction applied. (d,e,f) Signal along each acquisition window acquired with heart variability (30 %). TI optimization method was applied with W=0.4

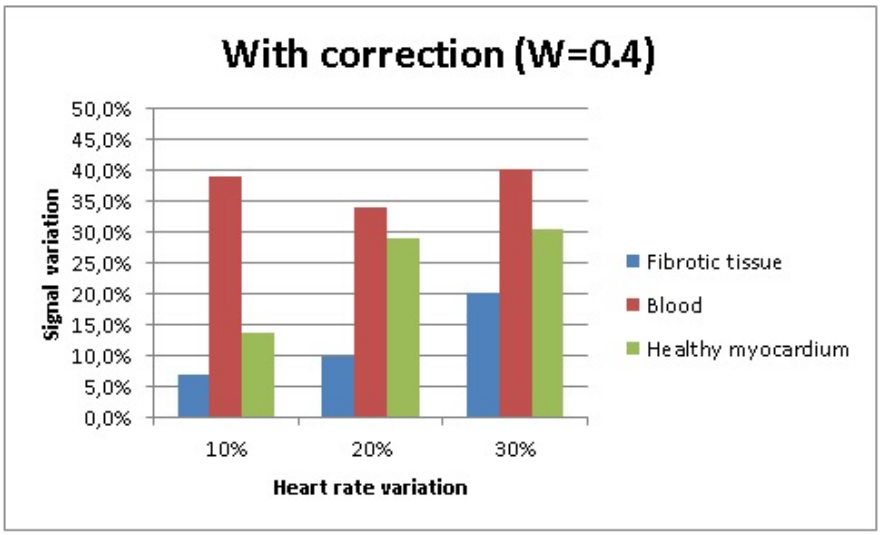

Figure 4.10: Measurements of signal variation (Y-axis) from phantom experiments as a function of heart rate variation (X-axis) with TI correction W=0.4 for the three tissue types.

Images acquired with different weighting factors showed congruent results to SI curves obtained with the same parameters.

For the application of the TI correction with W=0, blood signal was corrected and artefacts mainly arise from healthy myocardium and fibrotic tissue (Fig. 4.11 (a)). On the other hand if W=1, healthy myocardium signal was corrected and artefacts arise from blood and fibrotic tissue (Fig. 4.11 (b)). Nevertheless, since myocardium T1 value could had been wrongly estimated, the signal was not completely corrected and some artefacts are still present. Image obtained with W=0.4 seems to present less artefacts than the previous two (Fig. 4.11 (c)).

Again in accordance with the signal intensity curves previously shown, the 2D images also show that a correction at W=0.4 creates more artefacts arising from the fibrotic tissue. This occurs because since just the blood and myocardium signals were considered for TI optimization, the fibrotic tissue signal is left completely uncorrected. Therefore the fibrotic tissue high SI was highly affected by the HR variations. In addition, it is important to keep in mind that the level of artefacts arising from the fibrotic tissue in a *in-vivo* image would also be influenced by the extension of the lesion within the heart. However, the fibrotic tissue usually covers a small extension compared to the healthy myocardium and thereby the artefacts would probably have less impact than in these

phantom images where all tissues have the same size. Nevertheless, it could also be added as another parameter into the multi-tissue correction approach. Further studies using in-vivo measurements are advisable to further analyse this aspect.

However, measurements (Fig. 4.8 (b)) showed that even with an increase in artefacts arising from the fibrotic tissue, the proposed multi-tissue TI correction method reduces image artefacts 20% to 45 % more than a single tissue approach, correcting for the blood or the myocardium respectively.

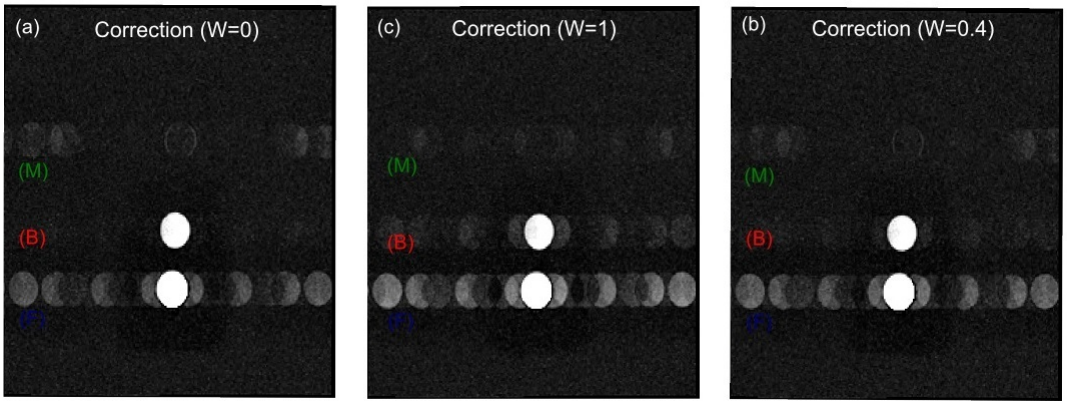

Figure 4.11: 2D images acquired at 3T using experimental phantoms representing fibrotic tissue (F), blood (B) and healthy myocardium (M). Images acquired with 30 % HR variations with: (a) TI correction applied with W=0 (correcting blood) (b)TI correction applied with W=1 (correcting healthy myocardium) (c) TI correction applied with W=0.4.

In conclusion, phantom experiments supported the conclusions obtained through simulation data. The novel multi-tissue TI optimization approach proved not only to greatly reduce image artefacts in general but to possibly overcome a TI correction where only the myocardium is corrected as in previous literature publications.

Chapter 5

Conclusions

DE-MRI has become a widely accepted tool in assessing several cardiac pathologies, being highly important when evaluating therapeutic course and prognosis of cardiac patients. A higher demand in medical applications motivated the research community to further improve image quality reducing image artefacts.

Within this context, this dissertation presented a novel method for reducing image artefacts in DE-MRI in patients with irregular heart rate.

A numerical simulation environment was built, allowing to model MR signal behaviour in a repeated IR DE-MRI acquisition. 2D images were also simulated using a virtual ECG signal, numerical phantom and analytic description of the MR signal behaviour during DE-MRI scans.

The simulation environment was validated with data acquired on a clinical 3T Philips scanner (Philips Healthcare, Best, The Netherlands). Simulation environment proved to be a good model of real DE acquisition.

The first goal of the project was to study the effect of irregular heart rate on MR signal behaviour and consequent image artefacts. This was accomplished both in simulated and scanner data. Signal behaviour simulated/acquired with a steady HR showed constant intensities over all cardiac cycles. On the other hand, signal behaviour with irregular HR showed strong variation.

A direct connection was established where a higher HR irregularity generates a more unsteady signal intensity behaviour. In addition, irregular HR also caused strong image artefacts both in simulated and acquired data. It was observed that HR irregularities

lead to a stronger signal deviation/image artefacts for the myocardium and blood signals rather than the fibrotic tissue.

The second and main goal was to develop a novel method to reduce image artefacts. A multi-tissue approach was presented where several tissues signal are corrected at the same time. The W factor allowed to correct more strongly for artefacts from blood (W<0.5) or myocardium (W>0.5). The W correspondent to the maximum artefacts reduction was determined to be equal to 0.4. The image acquired with W=0.4 correction showed less artefacts than the ones acquired with W=0 and W=1 (only one tissue corrected).

Simulation data measurements showed that, for a 30% HR variation, our multi-tissue TI optimization method reduced overall artefacts by more than 70 % compared with a non-corrected image. Moreover it reduced artefacts 20 to 30 % more than a single-tissue approach where only the blood or the myocardium are corrected individually.

Experimental data also showed improvement in image quality. The multi-tissue approach reduced artefacts by 20% compared to correcting for only the blood (W=0) and more than 45% when correcting for only the healthy myocardium (W=1).

In conclusion, this novel correction method not only has proven to greatly improve DE image quality but also to possibly overcome previous literature methods where only the healthy myocardium is corrected.

Results obtained in this study contributed to the scientific community aiming at improving DE image quality. A poster and oral presentation were presented at the European Society for Magnetic Resonance in Medicine and Biology (ESMRMB) 2013 congress, held in Toulouse (France) in October 2013.

Despite the positive results obtained with this study, some limitations were present. Inaccurate estimation of the T1 times of the gel phantoms could have led to a deviation between simulated and phantom experiments data. Further research in the subject is necessary in order to test T1 values of the phantoms, parameters used in the simulation and implementation in *in-vivo* image acquisition. Aspects as varying the mean heart rate to higher and lower values, testing different K-space sampling trajectories and gating methods could be interesting to study in the future. In addition, determination of the optimal W factor for *in-vivo* imaging is necessary.

Bibliography

[1] A. Arai P. Kellman. Cardiac imaging techniques for physicians: late enhancement. *Journal of magnetic resonance imaging*, 36(3):529–542, September 2012.

[2] R. Judd R. Kim, D. Shah. How we perform Delayed Enhancement imaging. *Journal of Cardiovascular Magnetic Resonance*, 5(3):505–514, May 2003.

[3] J S Detsky, J a Stainsby, R Vijayaraghavan, J J Graham, a J Dick, and G a Wright. Inversion-recovery-prepared SSFP for cardiac-phase-resolved delayed-enhancement MRI. *Magnetic resonance in medicine : official journal of the Society of Magnetic Resonance in Medicine / Society of Magnetic Resonance in Medicine*, 58(2):365–72, August 2007.

[4] L. Hsu Y. Chung O. Simonetti E. McVeigh A. Arai P. Kellman, A.C. Larson. Motion-corrected free-breathing delayed enhancement imaging of myocardial infarction. *Magnetic resonance in medicine*, 53(1):194–200, January 2005.

[5] J. Post G. Yo J. Verwoerd L. Kroft A. Roos H. Van den Bosch, J. Westenberg. Free-breathing MRI for the assessment of myocardial infarction: clinical validation. *AJR. American journal of roentgenology*, 192(6):W277–81, June 2009.

[6] R. Kim F. Saremi, J. Grizzard. Optimizing cardiac MR imaging: practical remedies for artifacts. *Radiographics : a review publication of the Radiological Society of North America, Inc*, 28(4):1161–1187, 2008.

[7] J. Burakiewicz. Artifact reduction in cardiac MRI in patients with varying heart rate. Master's thesis, 2010.

[8] J. Smink B. Cheong R. Muthupillai R. Krishnamurthy, A. Pednekar. Arrhythmia insensitive inversion recovery preparation (IR-prep)with real-time adaptive inversion delay (TI):phantom validation. *Journal of Cardiovascular Magnetic Resonance*, 12:168, 2010.

[9] G. D. Charles-Edwards T. Schaeffter J. Burakiewicz, C. Kolbitsch. Reducing artefacts inversion recovery prepared MRI caused by varying heart rate through real-time adaptation of the inversion time. *In the Proceedings of the 19th Annual Meeting of ISMRM*, page 4620, 2011.

[10] K. Kissinger B. Goddu S. Berg W. Manning R. Nezafat S. Weingärtner, M. Akçakaya. Combined saturation/inversion recovery sequences for improved evaluation of scar and diffuse fibrosis in patients with arrythmia or heart rate variability. *Proceedings of the 21st Annual Meeting of ISMRM 2013*, page 257, 2013.

[11] M. Roth J. Goldfarb, S. Arnold. Gadolinium pharmacokinetics of chronic myocardial infarcts: Implications for late gadolinium enhanced infarct imaging. *Journal of magnetic resonance imaging : JMRI*, 30(4):763–770, October 2009.

[12] V.D. Köchli D. Weishaupt. *How Does MRI Work ? An Introduction to the Physics and Function*. Springer, 2006.

[13] World Health Organization. The top 10 death causes in the world, August.

[14] National hear lung institute. What is coronary heart disease, August 2013.

[15] B. Knowles. *The Visualisation and Characterisation of Cardiac Lesions using Magnetic Resonance Imaging* . PhD thesis, 2010.

[16] K. Wu J. Vogel-claussen, C. Rochitte. Delayed Enhancement MR Imaging : utility in myocardial assessment. *Radiographics*, 26:795–811, 2006.

[17] Hajime Sakuma. Magnetic resonance imaging for ischemic heart disease. *Journal of magnetic resonance imaging*, 26(1):3–13, July 2007.

[18] T.A. Holly A. Wagner, H. Mahrholdt. Ce-mri and routine single photon emission computed tomography (spect) perfusion imaging for detection of subendocardial myocardial infarcts: an imaging study. *Lancet*, 361:374–379, 2003.

[19] A. Rafael R.J. Kim, E. Wu. The use of contrast-enhanced magnetic resonance imaging to identify reversible myocardial dysfunction. *N Engl J Med*, 343:1445–1453, 2000.

[20] E.L. Chen J.W. Lomasney K.J. Klocke R.M. Judd D.S. Fieno, R.J. Kim. Contrast-enhanced magnetic resonance imaging of myocardium at risk: distinction between reversible and irreversible injury throughout infarct healing. *J Am Coll Cardiol*, 36:1985–1991, 2000.

[21] W.G. Rehwald T. Albert R.J. Kim M.J. Robert, A. Wagner. Technology insight: assessment of myocardial viability by delayed-enhancement magnetic resonance imaging. *Nat Clin Pract Cardiovasc Med*, 2:150–158, 2005.

[22] T.B. Parrish K. Harris E.L. Chen O. Simonetti J. Bundy J.P. Finn F. Klocke R.M. Judd R.J. Kim, D.S. Fieno. Relationship of MRI Delayed Contrast Enhancement to irreversible injury, infarct age and contractile function. *Circulation*, 100(19):1992–2002, November 1999.

[23] Schulz-Menger J H. Abdel-Aty H, Zagrosek A. Delayed enhance- ment and t2-weighted cardiovascular magnetic resonance imaging differentiate acute from chronic myocardial infarction. *Circulation*, 109:2411–2416, 2004.

[24] G. Gubernikoff G-J.D. Vargas M. Parker R.M. Judd K.M. Choi, R.J. Kim. Transmural extent of acute myocardial infarction predicts long term improvement in contractile function. *Circulation*, 104:1001–1007, 2001.

[25] D.A. Bluemke K.C. Wu J.A. Lima B.L. Gerber, J. Garot. Accuracy of contrast-enhanced magnetic resonance imaging in predicting improvement of regional myocardial function in patients after acute myocardial infarction. *Circulation*, 106:1083–1089, 2002.

[26] Pound Bloembergen, Purcell. Relaxation effects in nuclear magnetic resonance absorption. *Phys Rev*, 73:679–712, 1948.

[27] M. Graves M. Prince D. McRobbie, E. Moore. *MRI From Picture to Proton*. Cambridge university press edition, 2006.

[28] J. Babb O. Simonetti V. Lee, Y. Chung. Myocardial infarction : optimization of inversion times at delayed contrast-enhanced MR imaging. pages 921–926, 2004.

[29] J. Weaver A. Stillman O. Simonetti R. White R. Setser, Y. Chung. Effect of inversion time on delayed-enhancement magnetic resonance imaging with and without phase-sensitive reconstruction. *Journal of magnetic resonance imaging : JMRI*, 21(5):650–655, May 2005.

[30] M. Frohlich R. Dietz J. Schulz-Menger D.R. Messroghli, A. Greiser. Optimization and validation of a fully-integrated pulse sequence for modified look-locker inversion-recovery (molli) t1 mapping of the heart. *J Magn Reson Imaging*, 26:1081–1086, 2007.

[31] D.C. Look. Time saving in measurement of NMR and EPR relaxation times. *Review of Scientific Instruments*, 41(2):250, 1970.

[32] W. Mützel H.J. Weinmann, M. Laniado. Pharmacokinetics of GdDTPA/dimeglumine after intravenous injection into healthy vol- unteers. *Physiol Chem Phys Med NMR*, 16:167–172, 1984.

[33] T. Holly M. Elliott R. Bonow-R. Kim R. Judd H. Mahrholdt, A. Wagner. Reproducibility of Chronic Infarct Size Measurement by Contrast-Enhanced Magnetic Resonance Imaging. *Circulation*, 106:2322–2327, 2002.

[34] J.R. Jones J. Mata B. French J.N. Oshinski, Z. Yang. Imaging time after Gd-DTPA injection is critical in using Delayed Enhancement to determine infarct size accurately with magnetic resonance imaging. *Circulation*, 104(23):2838–2842, December 2001.

[35] R. Busse S. Majumdar X. Li, E. Han. In vivo T1 mapping in cartilage using 3D magnetization-prepared angle-modulated partitioned k-space spoiled gradient echo

snapshots (3D MAPSS). *Magnetic resonance in medicine*, 59(2):298–307, March 2008.

[36] WolframAlphaMathWorld. Standard deviation, September 2013.